Thomas Köpplmayr

Photolithographic Micro-patterning of Polymers for Optical Applications

---

Supervisors:
Univ.-Ass. DI Dr. Thomas Grießer
Univ.-Prof. Mag. Dr. Wolfgang Kern

Master Thesis
Institute of Chemistry of Polymeric Materials
Chair of Synthesis of Special and Functional Polymers
Montanuniversität Leoben

I am among those who think that science has great beauty. A scientist in his laboratory is not only a technician: he is also a child placed before natural phenomena which impress him like a fairy tale. We should not allow it to be believed that all scientific progress can be reduced to mechanisms, machines, gearings, even though such machinery also has its beauty.

Neither do I believe that the spirit of adventure runs any risk of disappearing in our world. If I see anything vital around me, it is precisely that spirit of adventure, which seems indestructible and is akin to curiosity.

MARIE SKŁODOWSKA CURIE (1867-1934)

Abstract

This work deals with the synthesis and characterization of photoreactive polymers and their potential application in optics and opto-electronics.

First, polymers bearing phenyl or naphthyl ester groups are investigated. These polymers are easily accessible by polymer analogous esterification of commercially available poly(4-vinylphenol). Both polymers, poly(4-vinylphenyl benzoate) (PVP-**BZ**) and poly(4-vinylphenyl 1-naphthoate) (PVP-**NA**), undergo a Fries rearrangement upon exposure to UV light. This leads to a change in the refractive index up to $\Delta n = +0.036$. Refractive index patterns can be generated using photolithographic techniques, as shown by optical microscopy using a phase contrast set-up for visualization. Patterned films of PVP-**BZ** and PVP-**NA** with a resolution of 1 µm are obtained by the use of a mask aligner.

The formation of hydroxyketone groups upon UV irradiation also provides the opportunity of selective post-exposure reactions, including the immobilization of different fluorescent dyes in the illuminated areas. In combination with lithographic processes fluorescence patterns with bright luminescence are obtained.

The difference in UV absorbance of these polymers can be employed for the design of a dual-layer assembly. This allows selective patterning of each layer by the choice of the specified wavelength. Thus, these materials are of interest for multi-layer optical data storage applications.

In addition, (±)endo,exo-bicyclo[2.2.1]hept-5-ene-2,3-dicarboxylic-bis-(4-thiocyanatomethyl)benzylester is synthesized and polymerized via ring-opening metathesis polymerization (ROMP). The attached SCN-groups undergo a conversion to NCS-groups upon UV irradiation. This provides the possibility of selective surface functionalization by physical mixing with a fluorene-based electroluminescent polymer followed by photolithographic patterning and post-modification with a fluorescent dye. Due to Förster resonance energy transfer (FRET), tuning of the emission color can be achieved.

Kurzfassung

Diese Arbeit beschäftigt sich mit der Synthese und Charakterisierung von photoreaktiven Polymeren und deren potentiellen Anwendungen in der Optik und Opto-Elektronik.

Zuerst wurden Polymere mit Phenyl- oder Naphthylestergruppen untersucht. Diese Polymere sind leicht zugänglich über polymeranaloge Veresterung von kommerziell erhältlichem Poly(4-vinylphenol). Beide Polymere, Poly(4-vinylphenolbenzoat) (PVP-**BZ**) und Poly(4-vinylphenyl-1-naphthylester) (PVP-**NA**) reagieren nach einer Photo-Fries Umlagerung unter Einwirkung von UV-Licht. Dies führt zu einer Brechungsindexerhöhung um bis zu $\Delta n = +0.036$. Unter Verwendung photolithographischer Methoden können Brechungsindexmuster generiert und durch Lichtmikroskopie im Phasenkontrastmodus sichtbar gemacht werden. Strukturierte Filme von PVP-**BZ** und PVP-**NA** bis zu einer Auflösung von 1 µm können mit Hilfe eines Mask Aligners erzeugt werden.

Die Ausbildung von Hydroxyketon-Gruppen unter Einwirkung von UV-Strahlung bietet außerdem die Möglichkeit selektive Nachbehandlungsreaktionen durchzuführen, wie die Immobilisierung von verschiedenen Fluoreszenzfarbstoffen in den belichteten Bereichen. In Kombination mit lithographischen Prozessen können Fluoreszenzmuster mit deutlich sichtbarer Lumineszenz erzeugt werden.

Der Unterschied in der UV-Absorption dieser Polymere kann für die Entwicklung eines Zweischicht-Aufbaus genutzt werden. Dies erlaubt eine selektive Strukturierung jeder Schicht unter Verwendung der jeweiligen Wellenlänge. Dadurch sind diese Materialien von Interesse für mehrschichtige optische Datenspeicher.

Zusätzlich wird (±)endo,exo-Bicyclo[2.2.1]hept-5-en-2,3-dicarboxy-bis-(4-thiocyanatomethyl)benzylester synthetisiert und durch ringöffnende Metathese-Polymerisation polymerisiert. Die enthaltenen SCN-Gruppen werden unter Einwirkung von UV-Licht zu NCS-Gruppen umgelagert. Dies bietet die Möglichkeit selektiver Oberflächenfunktionalisierung durch physikalisches Mischen mit einem auf Fluoren basierenden, elektrolumineszenten Polymer, gefolgt von photolithographischer Strukturierung und Nachbehandlung mit einem Fluoreszenzfarbstoff. Durch Förster Energietransfer kann so die Emissionsfarbe eingestellt werden.

Acknowledgement

I greatly appreciate the help of my supervisors Univ.-Ass. Dr. Thomas Grießer and Univ.-Prof. Dr. Wolfgang Kern who advised and encouraged me during the compilation of this thesis.

I would like to thank the following people for participating in this project: Dr. Georg Jakopic (Institute for Surface Technologies and Photonics, Johanneum Research, Weiz) for the ellipsometric measurements, Dr. Massimilano Cardinale (Institute for Environmental Biotechnology, Graz University of Technology) for performing the confocal fluorescence microscopy, and Dr. Thomas Rath (Institute of Chemistry and Technology of Materials, Graz University of Technology) for instruction and assistance in preparing the OLEDs.

Moreover, many thanks go to Univ.-Doz. Dr. Gregor Trimmel (Institute of Chemistry and Technology of Materials, Graz University of Technology) for the thermal characterization of the polymers, as well as to Thomas Ehgartner (Polymer Competence Center Leoben GmbH) for the GPC measurements.

Special thanks go to all my colleagues at the Institute of Chemistry of Polymeric Materials for giving me advice during the practical work in the laboratory.

Financial support by the Austrian Science Fund (FWF) in the framework of a national network (NFN Interface controlled and functionalized organic films - project: S9702-N08 "*Design and application of tunable surfaces based upon photoreactive molecules*") is greatfully acknowledged. Part of this work was performed at the Polymer Competence Center Leoben GmbH (PCCL) within a strategic research project. PCCL is funded by the Austrian Government and the State Governments of Styria and Upper Austria within the COMET program.

Contents

Chapter 1

Motivation and Objective

Photolithographic techniques are widely used as tools to pattern thin films for electronic applications. It represents an adaptation of much older photo-based methods used in the graphic arts as early as the 1800s. In the most general sense, a photo-patterning process starts by coating a substrate with a material having properties that can be changed by exposure to light. Patterned exposure is most commonly achieved by passing light through a rigid mask that manipulates the phase and/or amplitude. The mask can be located in direct contact with (contact mode) or in proximity to (proximity mode) the photosensitive material. Alternatively, imaging optics can magnify or demagnify the mask image and project it onto this material (projection mode). [1]

Many examples of organic electronic and optoelectronic devices use photolithography to pattern the electrodes, dielectrics, encapsulating layers, and other elements. In these systems care is taken to develop processing sequences and material choices that yield device properties that are not degraded by the photolithographic process steps.

Electroluminescent conductive polymers emit light when connected to an external voltage. In turn, this molecular property is a consequence of the presence of multiple π-bonds. Such polymers are frequently used as emissive layers in organic light emitting diodes (OLEDs) and can be applied to a flexible substrate such as PET [2] by techniques derived from commercial inkjet printing. [3, 4] Thus, flexible displays may be produced inexpensively.

The use of polymeric materials as active elements for the construction of electronic devices, is rapidly expanding. In addition to light emitting diodes, polymeric materials have been used in the fabrication of many electronic compo-

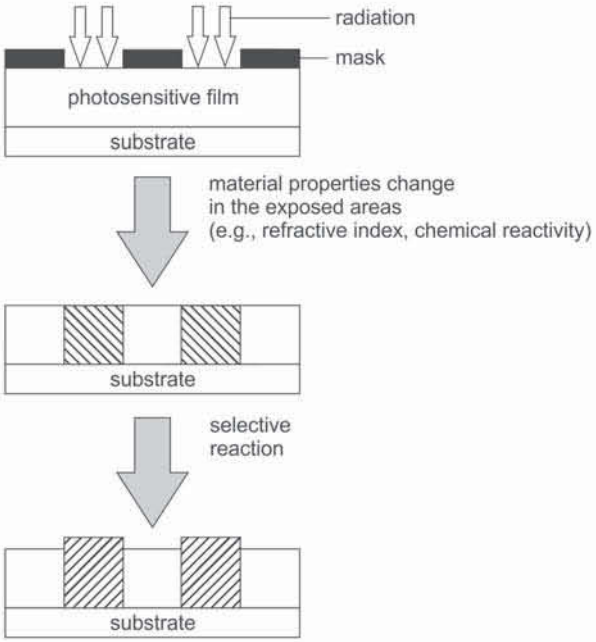

Figure 1.1: Basic principle of a photolithographic process.

nents: lasers [5], photovoltaic cells [6, 7], field effect transistors [8] and memory devices [9]. Consequently, it is possible to combine the good mechanical and processing properties of polymers with semiconducting behavior. Improving the performance of these devices by the creation of micrometric ordered patterns, is the object of much interest.

Photolithography in polymeric materials consists of several steps, as shown in Figure 1.1. First, the photosensitive film is illuminated using a mask to create irradiated and non-irradiated areas within the polymer. As a consequence, patterning of some material properties occurs, i.e., refractive index, adhesion or chemical reactivity.

Furthermore, various kinds of post-treatments may be used to modify the polymeric surface and meet specific requirements. When the patterned film is exposed to solutions or vapors of suitable chemicals, functional molecules like biomolecules, electroactive molecules or fluorescent dyes can be immobilized either in the illuminated or in the non-illuminated areas.

In fluorescent optical memories, fluorescent molecules are distributed within a polymer host. Lasers are used to induce chemical reactions at the spot and

multiple layer assemblies can be realized using non-photosensitive materials in between. Confocal configurations allow every layer to be read out separately.

In contrast to other optical data storage techniques, in fluorescent multilayer storage (FMS) the substrate, when it is read out by a laser beam, emits fluorescent light at a different wavelength. Thus, interference between light beams can be avoided. [10]

The present work focuses on the photo-Fries rearrangement of functional polymers bearing fully aromatic aryl ester units in the side chain. In particular, the photo-induced reactions in thin films of poly(4-vinylphenyl benzoate) (PVP-**BZ**) and poly(4-vinylphenyl 1-naphthoate) (PVP-**NA**) are investigated and the versatility of the photo-Fries reaction with respect to (i) refractive index modulation (ii) immobilization of fluorescent dyes in the illuminated areas is demonstrated. Both polymers are easily accessible by a polymer analogous reaction using the commercially available poly(4-vinylphenol) as starting material. This provides a convenient way for the synthesis of polymers with tunable refractive index as required for numerous optical applications.

Moreover, the application of these materials for novel multilayer data storage devices will be discussed. Due to the fact that the synthesized polymers exhibit different light absorption behaviours it is possible to achieve a selective writing in each layer of a sandwich assembly of both polymeric films via UV light of different wavelengths. This writing process can be performed without loss of power and without the demand of two-photon excitation.

In addition, (±)endo,exo-bicyclo[2.2.1]hept-5-ene-2,3-dicarboxylic-bis-(4-thiocyanatomethyl)benzylester (NOR-**SCN**) is synthesized and polymerized via ring-opening metathesis polymerization (ROMP). The photoisomerization reactions of benzyl thiocyanate moieties in thin polymeric films lead to a change of both the refractive index and the chemical reactivity in the illuminated areas.

Therefore, a highly fluorescent Ru(II) complex can be immobilized in the illuminated areas of this polymer and the possibility to use this approach for color-tuning of organic light emitting diodes is demonstrated. For that reason a blend of polyfluorene and PNOR-**SCN** has been applied as photoreactive emission layer. In order to achieve a tuning of the electroluminescence of such OLEDs, the Förster resonance energy transfer (FRET) from the conjugated polymer (i.e., polyfluorene) to the immobilized Ru(II) complex can be exploited.

Chapter 2

Introduction

2.1 UV induced reactions in polymer side groups

2.1.1 The thiocyanate – isothiocyanate conversion

Benzyl thiocyanate groups undergo a photoisomerization to benzyl isothiocyanate groups when being exposed to UV light. The reaction follows a radical mechanism and is irreversible (Figure 2.1). [11]

An irradiation of polymers bearing benzyl thiocyanate groups in the side chains leads to a change in the refractive index. In thin films of poly(4-vinylbenzylthiocyanate) an increase of $\Delta n = +0.03$ was observed. [12, 13]

Due to the different reactivity of thiocyanate and isothiocyanate groups the polymer surface can be modified. In the illuminated areas molecules bearing amine groups can be bound under the formation of derivatives of thiourea. [11]

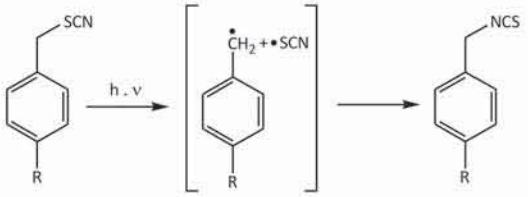

Figure 2.1: Isomerization of benzyl thiocyanate groups under exposure to UV light.

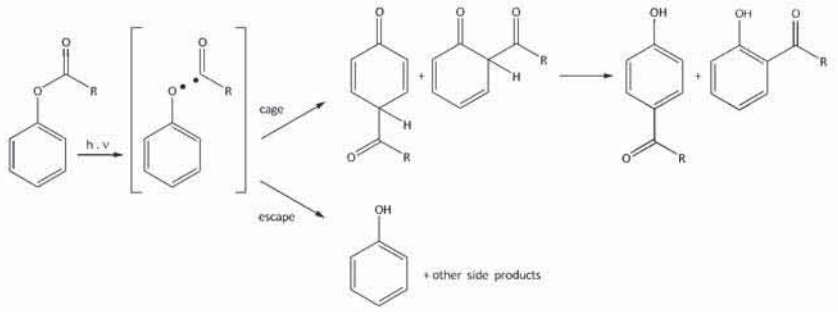

Figure 2.2: Mechanism of the Photo-Fries rearrangement.

2.1.2 Photo-Fries rearrangement of aryl esters

The photo-induced Fries reaction, the so called photo-Fries rearrangement, was first discovered by Anderson and Reese. [14] Aryl esters are transformed to hydroxyketones via free radical intermediates under exposure to UV light. The generally accepted mechanism [15, 16] is depicted in Figure 2.2.

Mechanistic investigations have been carried out by Lochbrunner et al. [17] The photolysis reaction mainly proceeds from the excited singlet (S_1) state. The photogenerated radicals can recombine and then yield a derivative of cyclohexadienone as the "cage product". The triplet pathway (from the T_1 state) of the reaction is of secondary importance and its contribution to product formation was reported to be less than 10 %. [18] Tautomerism then gives the hydroxyketone, which is the rearranged acyl migration product. [19]

The reaction is not limited to aryl esters. Corresponding photoreactions have been described for aryl amides, carbonates, carbamates, sulfonates, and sulfamates as well as for anilides, sulfonanilides, and sulfenanilides, as reviewed by Miranda and Galindo. [16]

First research on the photo-Fries rearrangement in polymers was done by Guillett et al. [20] who focused on the mobility of the radicals in poly(phenyl acrylate) and its effect on the distribution of the products. They were able to show that due to the limited mobility of the radicals mainly the *ortho*-product is formed.

It is less well known that UV illumination of aryl esters also yields decarboxylation products, see Figure 2.3. Decarboxylation was first observed by Finnegan and Knudsen. [21] This reaction also proceeds from the excited S_1 state and transforms the aromatic ester R-COO-R' into a hydrocarbon R-R'.

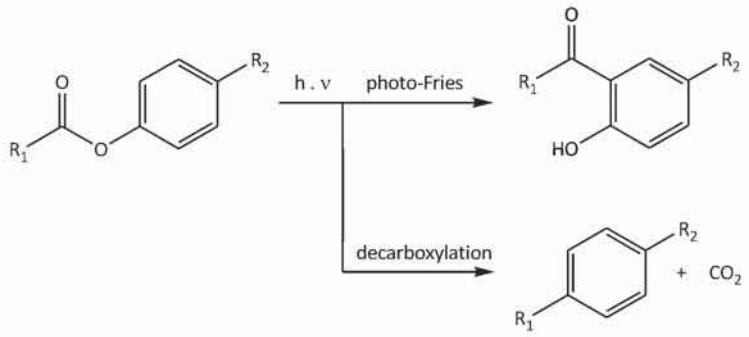

Figure 2.3: Two major routes for the reaction of aromatic esters upon UV irradiation: photo-Fries reaction and photoextrusion of CO_2 (decarboxylation).

For the photoextrusion of CO_2 a concerted mechanism has been proposed. It is known that steric hindrance of the ester and solvent effects can enhance the yield of the decarboxylation product. Templating effects have been observed by Weiss et al. [22]

The limited mobility of aromatic esters dissolved in a polymeric matrix leads to an enhanced yield of the photo-decarboxylation product, and at the same time the yield of the Fries rearrangement is lowered. [16]

In polymeric materials the reaction leads to an increase in the surface polarity due to the formation of the polar aromatic hydroxyl groups, as shown by Temmel et al. using the example of poly(acetoxystyrene). [23] In addition, the refractive index changes as well. Consequently, these types of photoreactive materials can be used for optical applications such as holographic data storage. [24]

The observed increase of the refractive index stems from the structural change in the chemical composition upon UV irradiation and is proportional to the conversion of the photoreactive groups, which allows a selective adjustment of the refractive index by the irradiation dose.

It has been demonstrated that a polymer bearing both naphthyl and phenyl ester groups provides the possibility of selective refractive index changes by the choice of the employed wavelength. [25] Due to the formation of different photoproducts depending on the irradiation wavelength and the irradiation sequence different refractive values could be adjusted in this polymer. Moreover, a two-step illumination procedure provides the possibility to erase and even invert the

index contrast generated during the first illumination step.

Furthermore, the UV absorbance can be adjusted. While polymers bearing phenyl ester groups absorb light up to $\lambda \approx 300$ nm, which is typical of the phenyl chromophore with its π-π^* transition, the UV absorption of polymers bearing naphthyl ester groups extends to 350 nm as expected for the naphthyl chromophore.

The photo-Fries rearrangement generally leads to stable photoproducts with high absorption in the UV region. [26, 20] Guilett et al. concluded that the enhanced stability of the rearranged products was partly due to their high absorption coefficients and partly due to their ability to dissipate the absorbed energy through non-photochemical pathways. [27] The formation of photostabilizing groups with high absorption coefficients (internal filter) leads to a decrease of the photoreaction during illumination up to a full stagnancy.

Moreover, the photo-Fries rearrangement in polymeric materials leads to a change in solubility. [28] Therefore, thin polymeric films have been applied as photoresists which can be developed both in positive or negative tone depending on the polarity of the developing solvent.

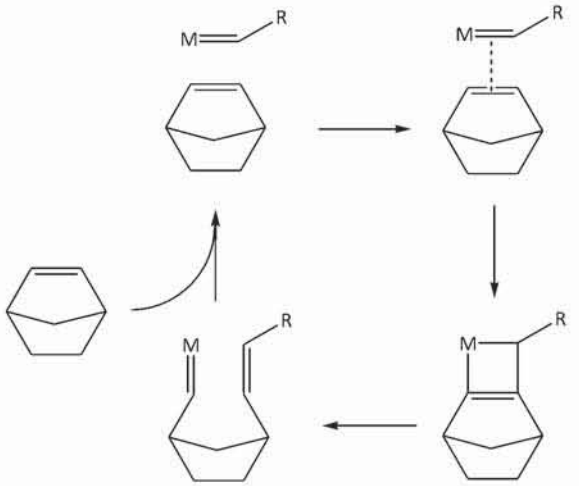

Figure 2.4: Mechanism of ROMP according to Hérisson and Chauvin.

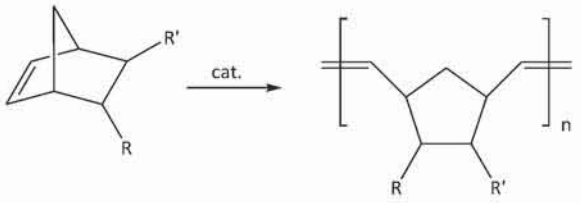

Figure 2.5: ROMP using the example of a derivative of norbornene.

2.2 Ring-opening metathesis polymerization

The mechanism of the ring-opening metathesis polymerization (ROMP) was first discovered by Hérisson und Chauvin in 1971 (Figure 2.4). [29]

The reaction is initiated by the addition of the olefin to the metal carbene of the catalyst. Consequently a metal cyclobutane ring is formed which is opened under the formation of two double bonds (Figure 2.5). The chain length can be adjusted by the ratio of monomer and catalyst. The catalyst is active until the end of the polymerization and creates polymers with low polydispersity index (PDI). This type of reaction is called a living polymerization. [30]

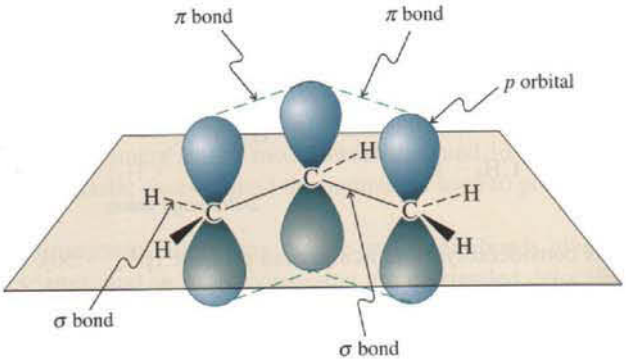

Figure 2.6: The three orbitals in the 2-propenyl (allyl) group overlap, giving a symmetric structure with delocalized electrons. [31]

2.3 Conjugated polyenes

2.3.1 Delocalization of electrons in conjugated dienes

Compounds containing carbon-carbon π-bonds, the products of overlap between two adjacent parallel p orbitals, undergo addition reactions to more complex products, including polymers. In this chapter the topic of compounds in which three or more parallel p orbitals participate in π-type overlap is discussed. The electrons in such orbitals are therefore shared by three or more atomic centers and are said to be delocalized.

The stabilization of the 2-propenyl (allyl) system by resonance can be described in terms of molecular orbitals. Each of the three carbons is sp^2 hybridized and bears a p orbital perpendicular to the molecular plane (Figure 2.6).

Conjugated dienes are more stable than non-conjugated dienes. The heat of hydrogenation of a terminal alkene is about -30 kcal.mol^{-1}. A compound containing two non-interacting terminal double bonds should exhibit a heat of hydrogenation roughly twice this value, about 60 kcal.mol^{-1}. [31]

$$CH_3CH_2CH = CH_2 + H_2 \rightarrow CH_3CH_2CH_2CH_3 \ \Delta H^0 = \text{-}30.3 \text{ kcal . mol}^{-1}$$

When the same experiment is carried out with the conjugated diene, 1,3-butadiene, a heat of hydrogenation about -57.1 kcal.mol^{-1} is produced. [31]

$$CH_2 = CHCH = CH_2 + 2\ H_2 \rightarrow CH_3CH_2CH_2CH_3 \ \Delta H^0 = \text{-}57.1 \text{ kcal . mol}^{-1}$$

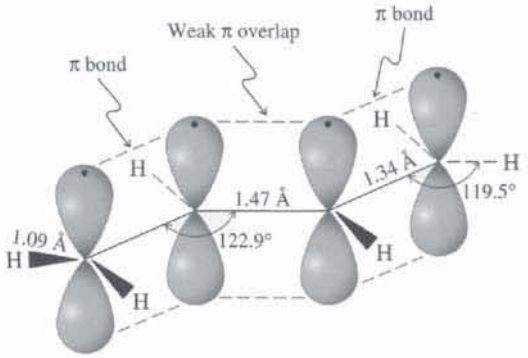

Figure 2.7: Structure of 1,3-butadiene. [31]

The difference, about 3.5 kcal.mol^{-1}, is based on a stabilizing interaction between the two double bonds. It is referred to as the resonance energy of 1,3-butadiene. [31]

The arrangement of the two double bonds permits the p orbitals on C_2 and C_3 to overlap. The π interaction is weak but nevertheless amounts to a few kilocalories per mole because the π electrons are delocalized over the system of four p orbitals (Figure 2.7).

The central bond is shorter than in an alkane (1.54 Å for the central C-C bond in butane). The p orbitals aligned perpendicularly to the molecular plane form a contiguous interacting array. [31]

2.3.2 Conducting polymers

In the late 1970s Heeger, MacDiarmid and Shirakawa synthesized a polymeric form of acetylene that conducts electricity. A conductive material has to provide electrons that are free to move and sustain a current, instead of being localized, as in most organic compounds. In conjugated polyenes such delocalization is attained by linking sp^2 hybridized carbon atoms in a growing chain.

Indeed, the electrons are still too "rigid" to move with the facility required for conductivity. To achieve this goal the electronic frame is "activated" by either removing electrons (oxidation) or adding them (reduction), a transformation called doping. The electron hole (positive charge) or electron pair (negative charge) delocalize over the polyenic structure. [31]

Because of its sensitivity to air and moisture, polyacetylene is difficult to

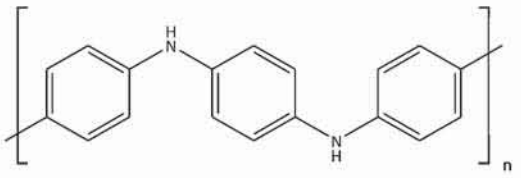

Figure 2.8: Polyaniline.

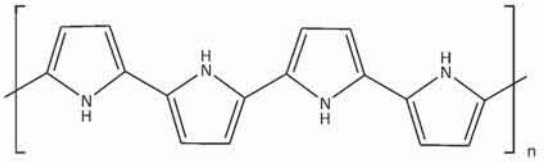

Figure 2.9: Polypyrrole.

use in practical applications. However, the idea of using extended π systems to impart organic conductivity can be exploited with a range of materials. Many of these contain especially stabilized cyclic 6π-electron units, such as benzene (Figure 2.8), pyrrole (Figure 2.9) and thiophene (Figure 2.10).

Apart from these applications in electronics, conducting polymers can be made to emit light when excited by an electric field, a phenomenon called electroluminescence that has gained enormous utility in the form of light emitting diodes (LEDs). [31]

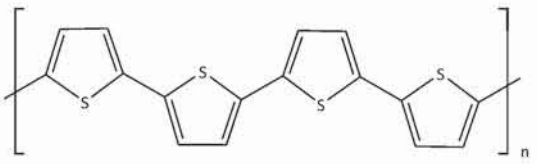

Figure 2.10: Polythiophene.

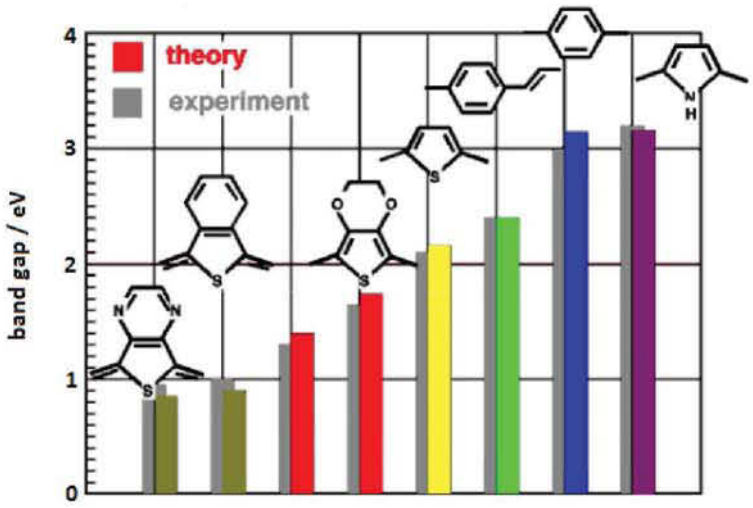

Figure 2.11: Band gap engineering and its effect on the emissive behavior of electroluminescent polymers. [35]

2.4 Organic Light Emitting Diodes (OLEDs)

2.4.1 Electroluminescent materials

Electroluminescence in organic semiconductors was first discovered by Pope et al. [32] in 1963. They observed emission from single crystals of anthracene, a few tens of micrometers in thickness, using silver paste electrodes. The process required large voltages to get emission, typically 400 V.

In 1983, electroluminescence of poly(vinyl carbazole) was reported [33] which led to a search for other electroluminescent polymers.

Due to the relatively poor lifetimes and low efficiencies traditional inorganic electroluminescent materials are still of great interest, since light-emitting devices (LEDs) based on these materials have been commercially available since early 1960s. The short lifetime is attributed to the rearrangement of the molecules caused by the heat generated, leading to crystallization. [34]

In the radiative process the energy of the released photon depends on the energy gap between the LUMO and the HOMO levels of the chromophore. For organic polymeric chromophores this energy gap ranges from 0.9 to 3.2 eV corresponding to light wavelengths covering the visible range, as shown in Figure 2.11.

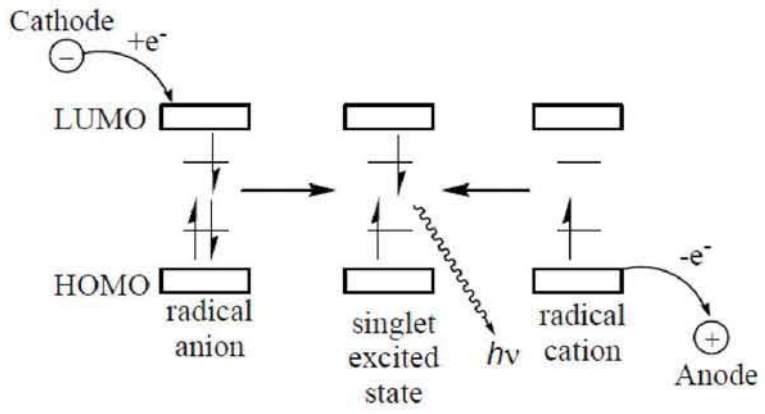

Figure 2.12: Energy diagram and layer sequence of an organic light emitting diode.

2.4.2 Functionality

An organic light emitting diode based on electroluminescent polymers consists of several layers: a hole transport layer (HTL), including a conducting polymer, and an electron transport layer (ETL), including an electroluminescent polymer, which are both incorporated between a cathode and a transparent anode placed on a substrate, typically made of glass or conventional polymeric materials.

The process responsible for the functionality of OLEDs requires the injection of electrons from one electrode and holes from the other, the capture of one by another, and the radiative decay of the excited state produced by this recombination process, as shown in Figure 2.12.

The cathode injects electrons in the conduction band of the polymer (π^* state), which corresponds to the lowest unoccupied molecular orbital (LUMO), and the anode injects holes in the valence band (π state), which corresponds to the highest occupied molecular orbital (HOMO).

The color of the emitted light is controlled by the band gap energy, while the charge injection process depends on the energy differences between the work functions of the respective electrodes and the electron affinity (cathode injection) as well as the ionization potential (anode injection) of the polymer. [34]

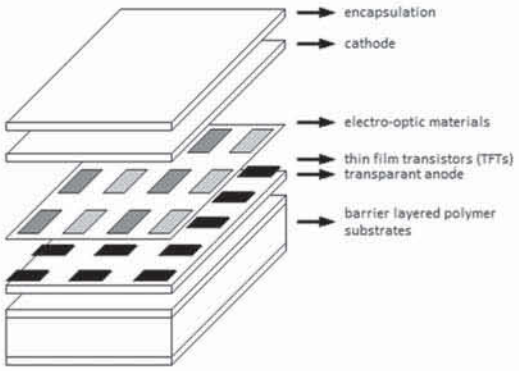

Figure 2.13: Cross-sectional structure of flexible displays.

2.4.3 Technology attributes and design aspects

Organic light emitting diodes are of great interest for flat panel displays. [36, 37, 5, 38] Polymers are very promising materials for flexible displays with many advantageous characteristics including transparency, light weight, flexibility, and robustness. Furthermore, they are some of the least expensive materials and are suitable for mass production.

Flexible OLEDs (FOLEDs) usually consist of a polymer substrate including some barrier-layers, a brittle transparent inorganic anode, a light-emitting layer, a layer containing thin film transistors (TFTs), a metal cathode, and some encapsulating layers, as shown in Figure 2.13. [39]

The key component to achieve flexibility is the substrate. Three kinds of substrates are considered to be flexible: thin glass, metal foil, and plastic. Thin glass films are bendable and have the highly desirable qualities of glass [40], although they are brittle, which limits their application as flexible substrates. Metal foils can also handle high process temperatures and provide a good barrier to moisture and oxygen, without the problems of breakability [41]. However, metal only works for non-transmissive displays and cannot handle multiple bends. In addition, it is an expensive material to use in large displays. Plastics is the material of choice, as it offers sufficient mechanical, optical, and chemical performance.

Currently, OLEDs are based on glass substrates because they are perfectly satisfactory for flat panel applications. The main fabrication steps are shown in Figure 2.14. [42]

To replace glass, a polymer substrate needs to have similar properties to

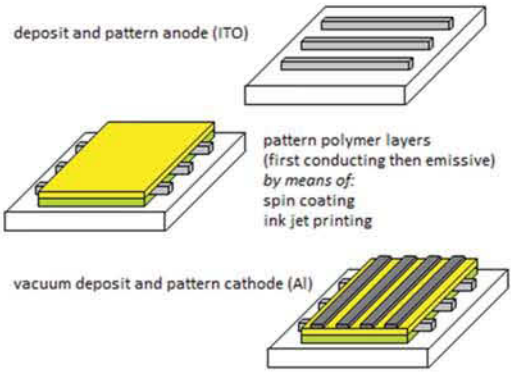

Figure 2.14: Polymer OLED display fabrication steps.

glass, including its clarity, dimensional stability, thermal stability, barrier properties, solvent resistance, low coefficient of thermal expansion (CTE), and smooth surface, as well as good optical properties [43, 44].

Thermoplastic semi-crystalline polymers available for flexible displays include polyethylene terephthalate (PET), polyethylene naphthalate (PEN), and polyetheretherketone (PEEK) [45, 46]. Polyesters such as PET and PEN have advantages with regard to clarity, coefficient of thermal expansion (CTE), chemical resistance, moisture absorption, and price while their upper operating temperature and surface roughness may not be sufficient for some applications.

There are two factors that have to be considered when selecting polymer materials with a proper thermal stability: CTE and the glass transition temperature (T_g), where the polymer chains start to move in order to relax the stress that is stored during the manufacturing process.

Conventional OLEDs can be classified by the kind of emitter material used in the device. Therefore, two types have been described, the Small Molecule Light Emitting Diode (SMOLED) and a second type made of macromolecules, better known as Polymer Light Emitting Diode (PLED). The main difference between them is the manufacturing technique employed for their production. SMOLEDs require chemical vapor deposition (CVD) techniques, which makes their production difficult and high-cost, whereas the fabrication of PLEDs usually includes coating techniques such as spin-coating, although sometimes photolithography is employed. [47]

For some polymer based OLEDs conventional photolithography is difficult because of material sensitivity and therefore, ink jet printing is an easy to apply

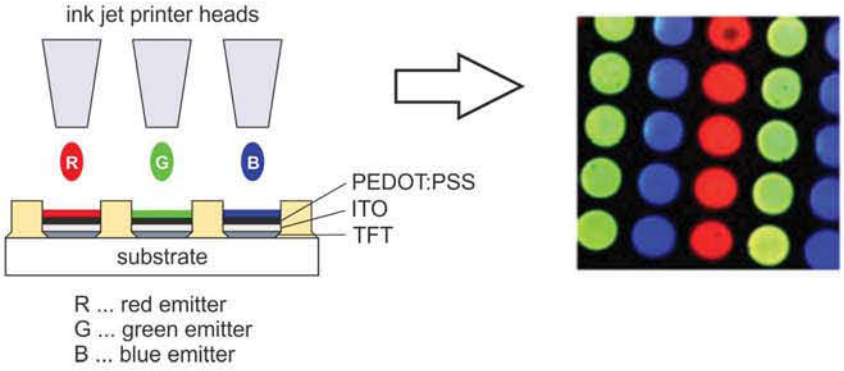

Figure 2.15: Ink jet printing to define and pattern red, green and blue emitting subpixels. [42]

and economic alternative for the fabrication of flexible displays (Figure 2.15).

Flat panel displays require electrically conductive and transparent electrodes, a challenge which can be overcome by using transparent conducting oxides (TCOs). Indium tin oxide (ITO) has been widely used as a transparent electrode material. ITO films show high optical transmittance of $>90\,\%$ in the visible light region and a low electrical resistivity ($2.10^{-4}\,\Omega$.cm) when deposited on glass substrates under optimized conditions. However, indium is one of the rarest materials and therefore, ITO films are very expensive. In addition, they are so brittle that they are not easy to apply to flexible displays. [39]

There have been some studies using ZnO instead because this material exhibits high optical transmission and good electrical conductivity accompanied by a lower prize. ZnO films with different doping systems were also investigated, such as Zr-doped ZnO thin films [48], Ti-doped zinc oxide thin films [49] and gallium-doped zinc oxide films [50].

Finally, OLEDs require almost perfect encapsulation against water and oxygen. Encapsulating layers must ensure impermeability to water vapor and oxygen during usage, which includes repeated bending in flexible displays, in particular.

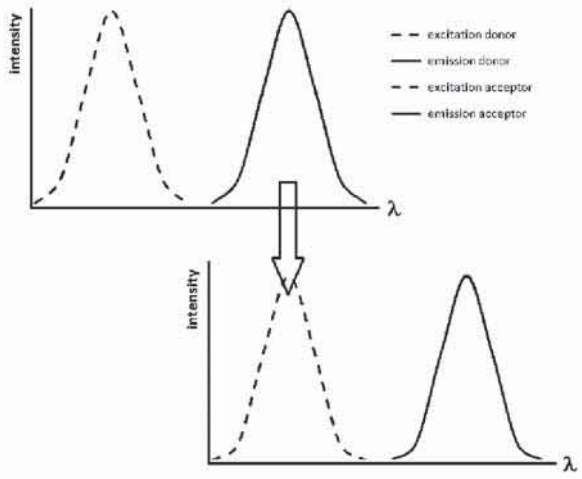

Figure 2.16: Energy transfer from an electroluminescent donor molecule to a fluorescent dye.

2.4.4 Color-tuning of OLEDs using Förster Resonance Energy Transfer (FRET)

Various methods of color-tuning in OLEDs are known in literature, including the use of organic chemistry to create homopolymers and copolymers with different molecular structures ("band gap engineering" methodology for semiconducting polymers) [51], the use of emitters in different amounts [52] and the use of a photoacid generator (PAG) for photo-induced quenching in the exposed areas. [53]

In the presence of two light-emitting materials energy transfer may occur, i.e., from an electroluminescent host-polymer to a fluorescent dye. If the emission spectrum of the donor and the excitation spectrum of the acceptor overlap, the original color of the device, given by the polymer, can be changed to the color of the light emitted by the fluorescent dye (Figure 2.16). Using photolithographic techniques, this approach can also be applied for color-tuning of OLEDs.

A similar method was presented by Trattnig et. al. [54] who focused on tuning of the energy transfer efficiency in a blend of conjugated polymers by using a blue emitting polyfluorene derivative as the host and a yellow emitting poly(para-phenylenevinylene) derivative as the guest material. By irradiating the blend with UV light in the presence of gaseous hydrazine the effective conju-

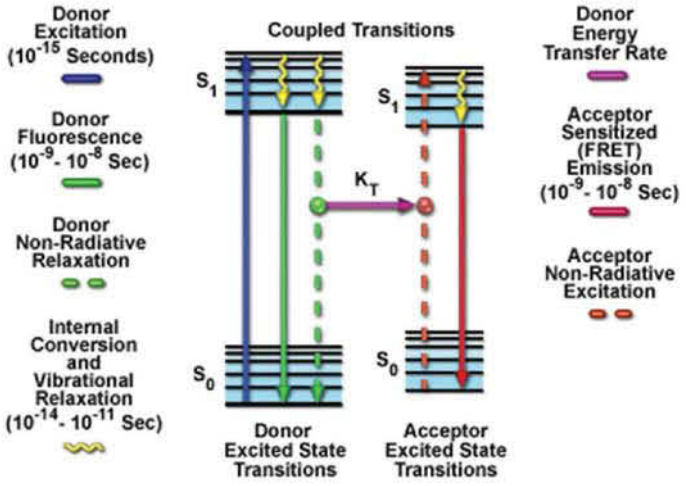

Figure 2.17: Electronic processes in a fluorescent host-guest systems. [58]

gation length of the guest could be reduced, which led to a shift in the absorption spectrum of the guest towards shorter wavelengths.

The electronic processes can be described with the classical Jablonski diagram, first proposed by Aleksander Jabłoński in 1935 to explain absorption and emission of light. [55]

When the donor molecule in its ground state (S_0^{D}) absorbs light, it is excited to a higher energy singlet state (S_1^{D}). The absorbed energy can be directly released via radiative decay or the molecule could be subject to collisions with the surrounding molecules, and undergo non-radiative decay processes to the ground state (or even decompose). In the presence of an acceptor molecule, energy transfer processes may occur, which brings the guest molecule to its first excited state and returns the host to the ground state. These processes may follow Förster, Dexter or radiative mechanisms. [56]

The Dexter mechanism describes an electron exchange and requires overlapping between the donor and acceptor orbitals. However, no spectral overlap is necessary and the energy transfer is limited to short ranges ($< 10\,\text{Å}$). [57]

In 1946 Theodor Förster published a paper in *Naturwissenschaften* dealing with the quantum-mechanical behavior of the transfer of electronic excitation energy between two molecules in a solution. He proposed a non-radiative mechanism which comes from long-range dipole-dipole interactions between the donor and the acceptor. According to his theory, the transfer arises from mutual

resonance dipole perturbations between the host- and the guest-molecule. [59]

Förster was interested in the topic because of the high efficiency in the photosynthetic process. He was aware from previous experiments, that leaves capture and use light energy much more effectively than it would be expected, even if photons hit the reaction centers precisely. [60]

The rate constant k of the Förster energy transfer is inversely proportional to the sixth power of the distance R between the molecules:

$$k = \left(\frac{R_0}{R}\right)^6 \cdot \frac{1}{\tau_D}$$

where τ_D is the lifetime of the donor excited state and the constant R_0 is the critical quenching radius (usually between 50 and 100 Å). [56]

In reality, one can observe the emission of the host molecule, the guest molecule, or a combination of both, depending on the efficiency of the energy transfer processes.

There are two fundamental requirements for efficient energy transfer via the Förster mechanism: (i) good spectral overlap between the emission of the donor and the absorption of the acceptor, and (ii) uniform mixing of the two species. Good mixing is required since the range of the energy transfer is only a few nanometers and the efficiency decreases with the sixth power of the distance, as mentioned before. [61]

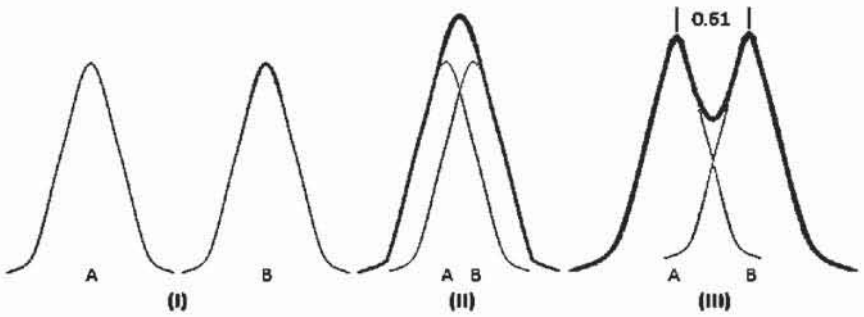

Figure 2.18: (I) The Airy disk intensity profile from two point sources A and B defines the resolution of a lens. In (II) the two Airy disks are so close that they cannot be distinguished, but in (III) the two are separated such that the maximum in the image of A overlaps the minimum in B. This is the definition of resolution defined by the Rayleigh criterion. [62]

2.5 Optical data storage

Commercial optical data storage usually includes a flat, circular disk which encode binary data in the form of "pits" (lower regions) and "lands" (higher regions) on a suitable storage medium. The encoding material sits atop a thicker substrate (usually polycarbonate) which makes up the bulk of the disk. The encoding pattern follows a continuous, spiral path covering the entire disk surface and extending from the innermost track to the outermost track. The data is stored on the disk with a laser or stamping machine, and can be accessed when the data path is illuminated with a laser diode in an optical disk drive.

The resolution of an optical imaging system is limited by various factors such as imperfections in the lenses or misalignment. All these kinds of limitations are referred to as optical aberrations. However, there is a fundamental maximum to the resolution of any optical system as well: Due to diffraction through the aperture of the external light source, which is used to illuminate the object, the electromagnetic waves form a diffraction pattern. The diffraction patterns, which have centers on points that are sufficiently close to each other, partly overlap.

The minimal distance s between two points A and B is therefore a function of the numerical aperture NA of the objective lens. According to the Rayleigh resolution criterion, this distance is given by: [63]

$$s = 1.22 \cdot \frac{\lambda}{2n \cdot \sin(\alpha)} = 0.61 \cdot \frac{\lambda}{NA}$$

where n is the refractive index of the medium between the objective lens and the object, λ is the wavelength of the light used to image the sample, and α is the half-angle of the maximum cone of light that can enter or exit the lens. The factor 1.22 is given by the radius of the first dark fringe in the Airy disk, the diffraction pattern associated with a circular aperture, as shown in Figure 2.18.

Present techniques have almost reached this limit in optical memories commercially sold as compact disks or magneto-optic disks. Even with an infinitely large objective lens, the best achievable bit-data resolution distance for recording and reading is limited by approximately half the beam wavelength.

In near-field optics, the problem of a diffraction-limited spot size experienced in conventional optics is overcome by placing the aperture close to the surface being studied and scanning the aperture across the surface in a raster pattern. By using this near-field aperture, the resolution could be determined by the size of the hole and not the wavelength of light. [63]

The scanning tunneling microscope (STM) follows a different principle: A mechanical probe is used rather than a hole and there is no external source to "illuminate" the surface. Instead, it uses electrons already present on the surface and the tip. In theory, the STM can have a resolution of an atom. However, the problem is that of vibration and environmental effects. [63]

One way of increasing the storage capacity is to use shorter wavelength lasers which allow smaller bit sizes to be obtained. Another way to increase the storage capacity is through the use of volumetric storage using holographic techniques.

In conventional photography only the intensity (squared amplitude) distribution of an object is captured while in holographic data storage the object phase variations, that carry the depth information, are recorded as well. The basic idea of holographic data storage was invented by D. Gabor in 1948 as a two-step lensless imaging technique to enhance the resolution of electron microscopy, for which he received the 1971 Nobel Prize in physics. [64]

However, the lack of a strong coherent light source was an essential drawback until the laser principle was introduced in the 1960s. In addition, volume holography was invented and opened the possibility of recording many holograms within the same physical volume which then could be retrieved independently thanks to a unique addressing scheme. Figure 2.20 shows a schematic readout system of a holographic disk.

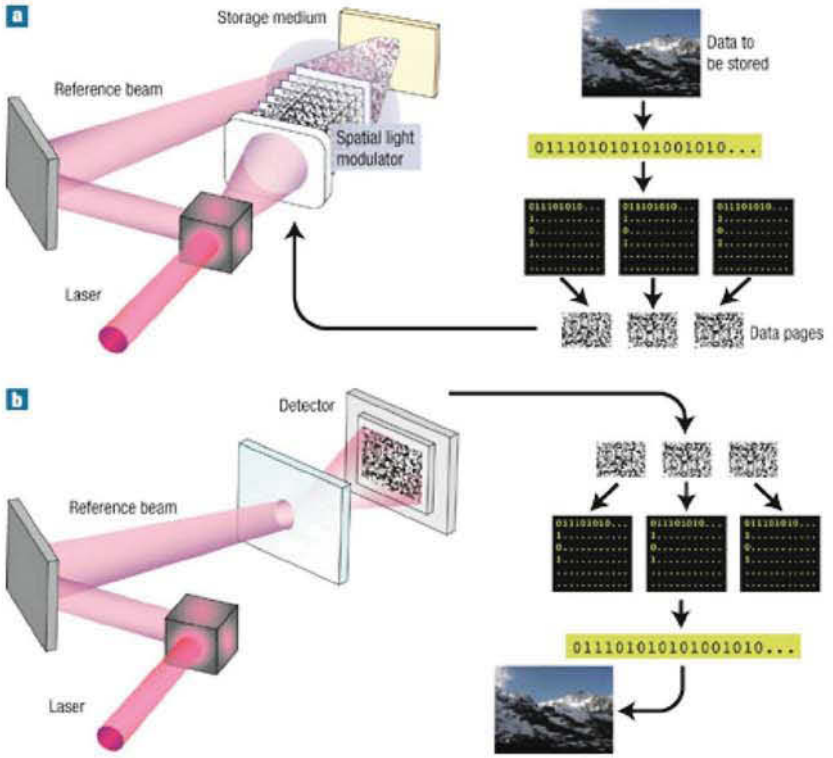

Figure 2.19: Holographic recording and reading processes. (a) The data are digitized, formed into pages of data with which the signal beam is modulated to write on the storage medium. (b) A reference beam is shone onto the storage medium and the modulation of the diffracted light is detected to reconstruct the original data. [65]

In holographic memories a coherent light from a laser source is collimated to produce a unit-amplitude plane wave normally incident on the object, while at the same time a spatial carrier reference wave illuminates the object as well. The stored data is read using the same reference beam used to create the hologram. The beam is focused on the photosensitive material, illuminating the appropriate interference pattern, the light diffracts on the interference pattern, and projects the pattern onto a detector which is capable of encoding the data. The recording and reading steps are illustrated in Figure 2.19.

Although images can clearly be stored in and retrieved from such holograms, the true potential of holographic data storage can be realized only when one considers utilizing the third dimension of the recording medium. A grating

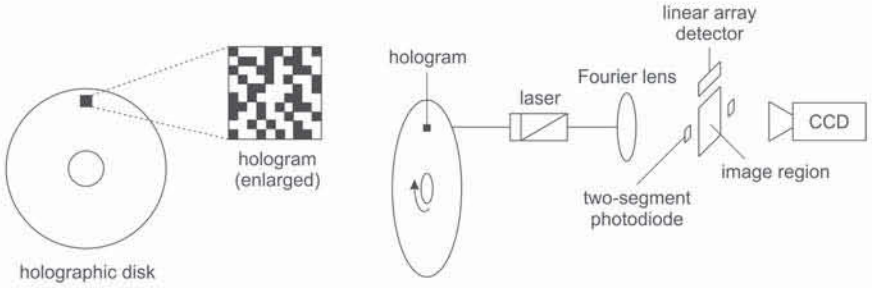

Figure 2.20: Stored model of optical disk holograms on the disk substrate (left). Schematic readout system of a holographic optical disk (right).

whose thickness significantly exceeds the fundamental fringe period recorded in it is said to operate in the Bragg diffraction regime, where the extended volume of the medium suppresses all but the first diffraction order in reconstruction. Consequently, it is possible to record many holograms within the same physical volume by using reference waves at angles at which no grating diffraction is observed. [64]

Various materials such as photopolymers, photorefractive crystals, photochromic materials, and polarization sensitive materials can be used to store data. Among them, photorefractive recording mediums in which data are stored as refractive index change are widely used, because they have little absorption so the light easily penetrates in deep layers in the medium.

In holographic data storage each recorded hologram uses up a certain portion of the total available refractive index change, and once the entire range is exhausted, no more holograms can be recorded. Therefore, the ultimate physical limit on the storage density is reached and the average diffraction efficiency is inversely proportional to n^2, which has been found empirically for a large number n of holograms. [64]

Holographic memories are able to satisfy the increasing demand for high capacity and fast-access data storage. To overcome the density limitation, bitwise multilayered optical memories are a promising alternative. Therefore, the data are recorded on concentric tracks in serial by focused spots within a thick volume. This approach requires an optical reading system that is able to read the data from a particular layer without cross talk between adjacent layers. Furthermore, a recording technique is essential which makes it possible to write information at a particular layer without erasing or corrupting the data already written at neighboring layers. [66]

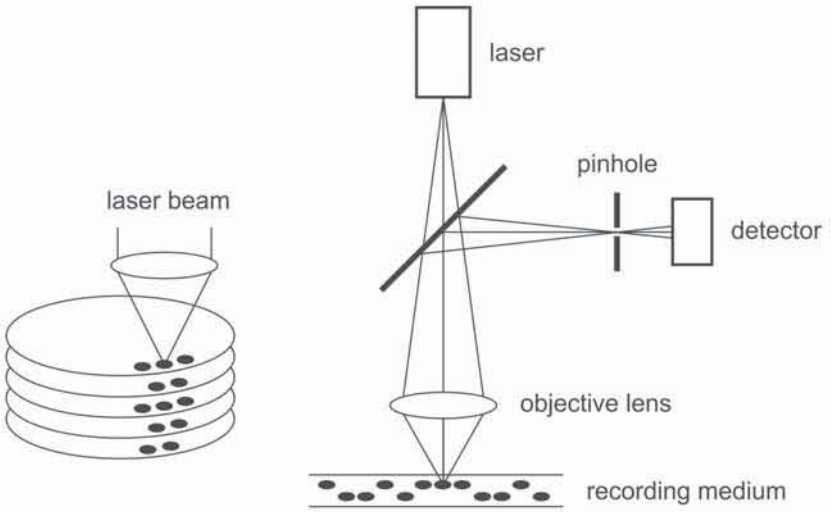

Figure 2.21: Confocal readout of multi-layered optical memory.

A typical readout system based on a reflection confocal microscope configuration is shown in Figure 2.21. The system gives high contrast, because the pinhole before the detector eliminates scattered light from out of the focus region.

In volumetric bitwise memories several techniques can be used to record data, including two-photon absorption [66] and the use of a recording medium in which photosensitive films and non-photosensitive films are placed alternately. [67]

One of the disadvantages of holographic data storage is that since the holograms are read from the same volume, cross talk effects may not be negligible. Furthermore, the reflected laser light has the same frequency as the read beam, so the two interfere with each other. Also, in bit-oriented three-dimensional memories high signal-to-noise ratios (SNR) are of great interest.

Fluorescent molecules can be distributed within the (polymeric) recording medium to overcome this problem. In contrast to other optical data storage techniques, in fluorescent multi-layer storage (FMS) the substrate, when it is read out by a laser beam, emits fluorescent light at a different wavelength. Thus, interference between light beams can be avoided. [10]

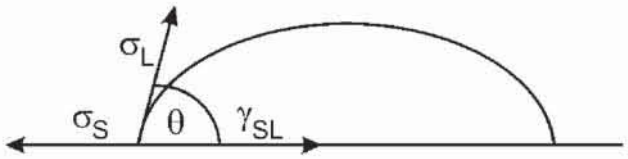

Figure 2.22: Contact angle of a droplet spread out on a solid surface.

2.6 Contact angle measurements

Contact angle measurements can be performed using the sessile drop method in combination with the theory of Owens-Wendt [68, 69] to calculate the surface energy of solid materials.

When a liquid gets in contact with a solid, an interface is formed. The interfacial tension γ_{SL} is given by the Dupré equation:

$$\gamma_{SL} = \sigma_S + \sigma_L - W_{adh}$$

σ_S and σ_L are the surface energies of the solid and the liquid, respectively. The adhesion work W_{adh} refers to the separation of the two phases to an infinite distance in vacuo. [70]

In contact angle measurements a three-phase system has to be investigated (Figure 2.22). At equilibrium the chemical potential in the three phases is equal and the following equation must be satisfied (known as Young's equation):

$$\sigma_S = \sigma_L \cdot \cos(\theta) + \gamma_{SL}$$

The contact angle ϑ is measured using the sessile drop method. The surface tension can be divided into a disperse and a polar part.

$$\sigma = \sigma^D + \sigma^P$$

Fowkes assumed there is just uniform interaction between the solid and the liquid phase, i.e., a disperse substance can only interact with the disperse part of the adjacent phase. [71] Using the geometric mean, the Dupré equation can be modified the following:

$$\gamma_{SL} = \sigma_S + \sigma_L - 2 \cdot \left(\sqrt{\sigma_S^D \cdot \sigma_L^D} + \sqrt{\sigma_S^P \cdot \sigma_L^P} \right)$$

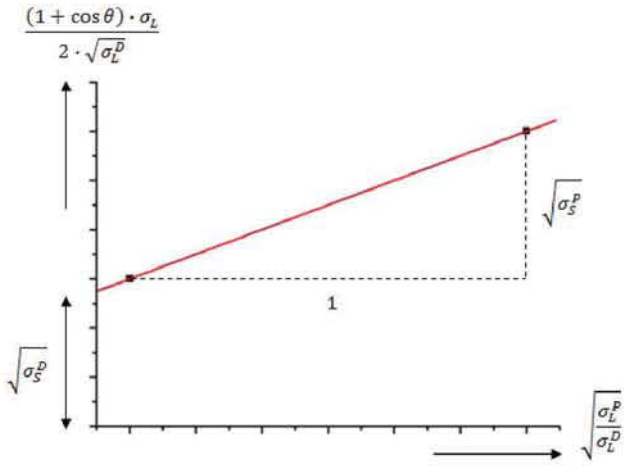

Figure 2.23: Calculating the surface energy from Owens-Wendt plot.

In combination with Young's equation a linear relation is obtained which can be used to calculate the disperse and the polar component of the surface energy as well as the polarity of the surface.

$$\frac{(1+\cos(\theta))\cdot\sigma_L}{2\cdot\sqrt{\sigma_L^D}} = \sqrt{\sigma_S^P}\cdot\sqrt{\frac{\sigma_L^P}{\sigma_L^D}} + \sqrt{\sigma_S^D}$$

With at least two test liquids a linear method can be used to determine the slope and the ordinate intercept as demonstrated in Figure 2.23. In many cases, water and diiodomethane are used to determine the surface energy of a solid surface.

Chapter 3

Results and discussion

3.1 Synthesis of the polymers

Four different polymers bearing photosensitive groups in their side chains have been synthesized. Table 3.1 gives an overview of the respective compounds.

The photoreactive polymers poly(4-vinylphenyl benzoate) (PVP-**BZ**), poly(4-vinylphenyl 1-naphthoate) (PVP-**NA**), and poly(4-vinylphenyl pyrene-1-carboxylate) (PVP-**PY**) are easily accessible by polymer-analogous reactions, as shown in Figure 3.1.

Starting from poly(4-vinylphenol) ($M_w = 13\,600\,g{\cdot}mol^{-1}$, PDI = 2.5), PVP-**BZ** was obtained by an esterification reaction using benzoyl chloride and a catalytic amount of pyridine. The preparation of PVP-**NA** was accomplished by using 1-naphthoyl chloride. Both polymers were obtained in a good yield of 83 % and 70 %. The polymers were characterized by ^{1}H-NMR, FT-IR and UV/VIS spectroscopy, and by GPC and DSC.

PVP-**PY** was obtained by esterification with pyrene-1-carbonyl chloride, which could be achieved by the reaction of pyrene-1-carboxylic acid with thionyl chloride. The polymer was only characterized by FT-IR spectroscopy as it turned out not to be suitable for photo-Fries type reactions.

PVP-**BZ** and PVP-**NA** showed excellent film forming properties when being spin-cast from dichloromethane solutions and fully transparent films with good optical quality were obtained. The glass transition temperatures are well above room temperature (PVP-**BZ**: 145.78 °C and PVP-**NA**: 89.11 °C). PVP-**PY** showed poor film forming properties due to its poor solubility in com-

Table 3.1: List of synthesized polymers.

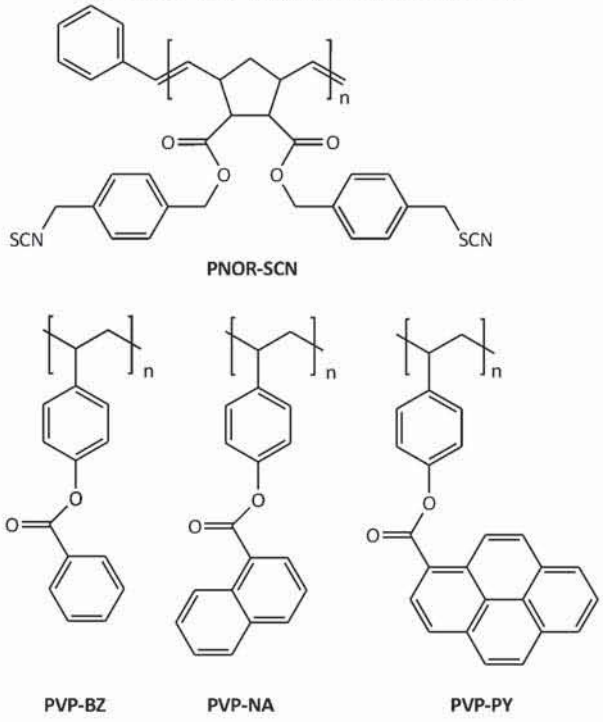

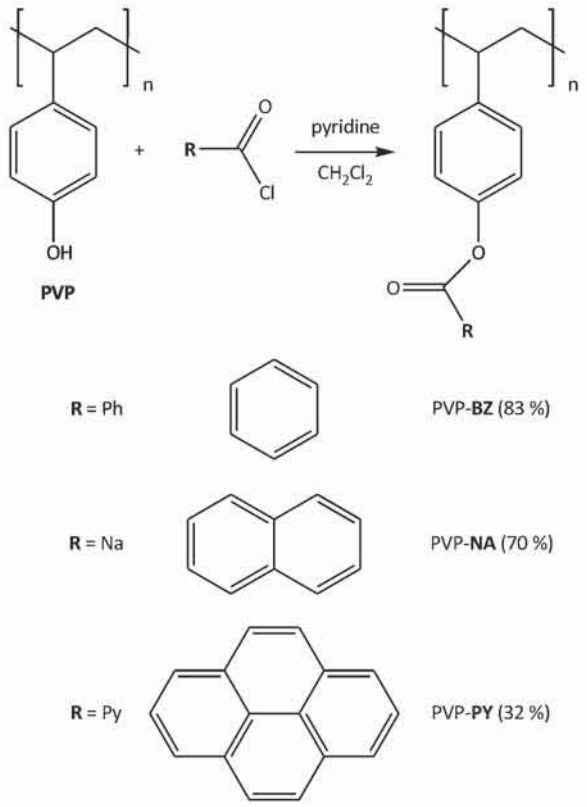

Figure 3.1: Synthesis of three different derivatives of poly(4-vinylphenol) by polymer-analogous esterification of PVP with the respective acid chloride.

mon organic solvents.

PNOR-**SCN** was obtained from its monomer (±)endo,exo-bicyclo[2.2.1]hept-5-ene-2,3-dicarboxylic-bis-(4-thiocyanatomethyl)benzylester which was synthesized by a two-step process starting from (4-chloromethyl)benzyl alcohol and adding (±)endo,exo-bicyclo[2.2.1]hept-5-ene-2,3-dicarbonyl dichloride in a second step as illustrated in Figure 3.2.

(4-Thiocyanatomethyl)benzyl alcohol was obtained in a good yield of 99 % as expected for a S_N2 reaction under given conditions. The second step required purification using column chromatography (cyclohexane / ethyl acetate 2/1) as a significant amount of different side products were formed. The polymer was characterized by ^{1}H-NMR, FT-IR and UV/VIS spectroscopy, and by GPC and DSC.

The yield of the ring-opening metathesis polymerization was comparably low and the polydispersity was higher than usual for this type of polymerization. Gel permeation chromatography (GPC) evidenced a polymer with a molecular weight M_n of about 22 200 g.mol^{-1} with a polydispersity index of 1.33 as measured against polystyrene standards. Under optimum conditions, the polydispersity index should be close to 1, meaning that every catalyst molecule reacts at the same time and with equal velocity until no monomer is left.

In general, polymerizations of nitrile containing monomers with ruthenium initiators are known to cause problems, due to strong interactions of the nitrile group with the metal center. [11]

DSC measurements showed a glass transition temperature at 39.10 °C. It was possible to cast homogeneous polymer films onto CaF_2 plates by spin coating from polymer solutions in dichloromethane.

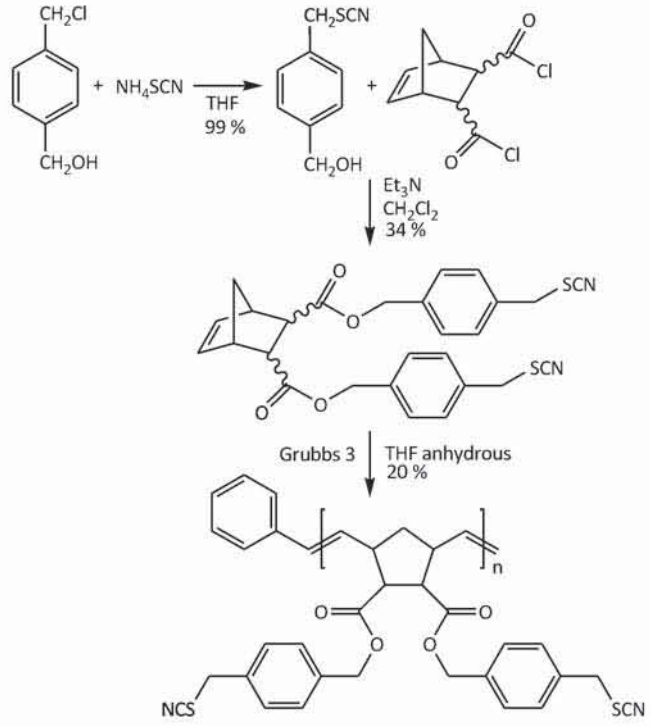

Figure 3.2: Synthesis of PNOR-**SCN** by a two-step process to obtain the monomer followed by ring-opening metathesis polymerization (ROMP) using Grubbs catalyst 3rd generation.

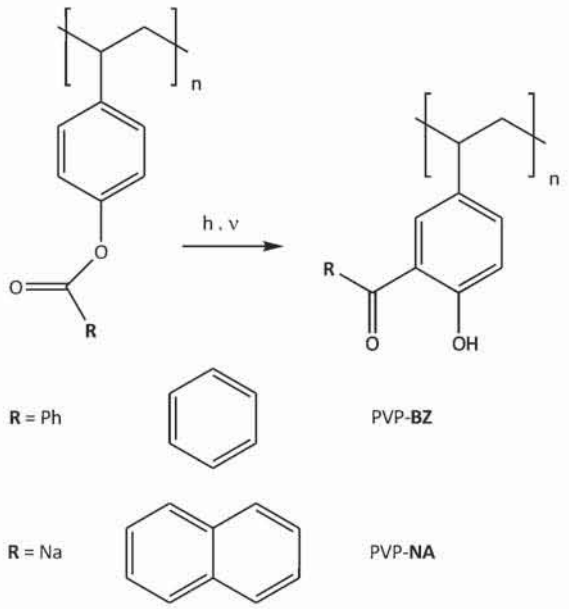

Figure 3.3: Photo-Fries rearrangement of PVP-**BZ** and PVP-**NA**.

3.2 Investigation of the photoreactions

3.2.1 Photoreactions of PVP-BZ and PVP-NA

Upon irradiation with UV light the photoreactive ester groups in PVP-**BZ** and PVP-**NA** undergo the photo-Fries rearrangement to give the corresponding *o*-hydroxyketones, as depicted in Figure 3.3. Because of this significant change in the chemical structure of the polymer's side chain, the photoisomerization can be easily followed by spectroscopic methods such as UV/VIS and FT-IR spectroscopy.

Figure 3.13a shows the UV spectra of PVP-**BZ** before and after illumination. The film absorbs light up to 300 nm with an absorption maximum localized at 230 nm. UV absorption in this range is typical of the phenyl chromophore with its π-π^* transitions. The ester group itself absorbs weakly around 190 nm (π-π^*) and with low absorbance around 270 nm (n-π^*), whereas the C=C double bonds absorb around 200 nm (π-π^* transition). An irradiation with UV light of 254 nm causes a significant increase of the absorbance in the range of 250 nm - 400 nm accompanied by the appearance of two maxima at 260 nm and 355 nm. These changes indicate the formation of aromatic hydroxyketone units

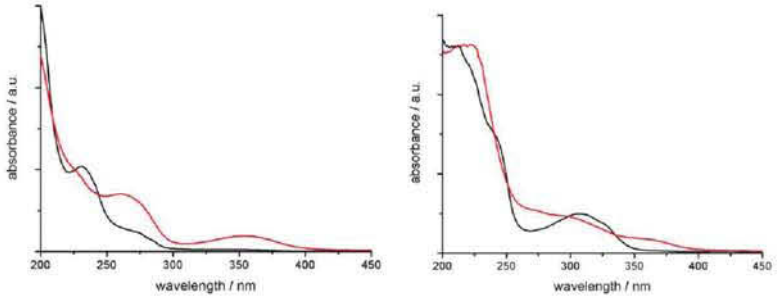

Figure 3.4: (a) UV/VIS spectra of PVP-**BZ** prior to (black line) and after illumination (red line). $\lambda = 254\,nm$; radiant energy per unit area $= 5.47\,J.cm^{-2}$ (b) UV/VIS spectra of PVP-**NA** prior to (black line) and after illumination (red line). $\lambda = 313\,nm$; radiant energy per unit area $= 2.22\,J.cm^{-2}$.

and are assigned to the π-π^* and n-π^* orbital transitions, respectively. In addition, a moderate decrease in absorbance below 250 nm and the depletion of the absorption maximum at 230 nm can be observed.

In a similar fashion the photoreaction of PVP-**NA** was studied. In this case, monochromatic irradiation of $\lambda = 313\,nm$ was used in these experiments. The UV absorbance spectra of PVP-**NA** before and after illumination are represented in Figure 3.13b. The film absorbs light up to 350 nm with an absorption maximum localized at 305 nm. Upon irradiation a moderate increase in the UV absorption in the range 210 nm - 240 nm and a significant increase in the range of 250 nm - 295 nm can be observed. In addition, the film absorbs light up to 400 nm while the maximum at 305 nm diminishes.

The photoreaction was followed by quantitative FT-IR spectroscopy which proved to be an appropriate tool because the functional group in the educt (i.e., the ester unit) and the functional group in the expected photo-Fries product (i.e., hydroxyketone) display well-resolved signals in the infrared spectrum. FT-IR spectra of the non-illuminated and the illuminated films of PVP-**BZ** and PVP-**NA** are shown in Figure 3.9. In the spectrum of the non-irradiated film the signal at about $1730\,cm^{-1}$ (C=O stretch) is typical of ester units. After UV irradiation, this vibrational band has considerably decreased. Instead, a new band evolves at $1630\,cm^{-1}$ which can be assigned to the formation of *o*-hydroxyketones. [72]

In order to obtain an insight into the reaction rate of the photo-Fries rearrangement, the FT-IR signals of the ester ($1730\,cm^{-1}$) and of the ketone

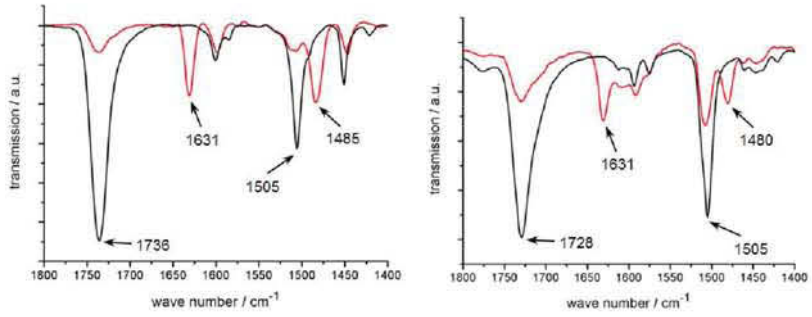

Figure 3.5: (a) FT-IR spectra of PVP-**BZ** prior to (black line) and after illumination (red line). $\lambda = 254\,\text{nm}$; radiant energy per unit area = $5.47\,\text{J}\cdot\text{cm}^{-2}$ (b) FT-IR spectra of PVP-**NA** prior to (black line) and after illumination (red line). $\lambda = 313\,\text{nm}$; radiant energy per unit area = $2.22\,\text{J}\cdot\text{cm}^{-2}$.

product ($1630\,\text{cm}^{-1}$) were evaluated. FT-IR spectra were recorded after different periods of UV irradiation and the carbonyl signals were integrated. Using the infrared absorbance coefficients of model compounds (phenyl benzoate: $700\,\text{L}\cdot\text{mol}^{-1}\cdot\text{cm}^{-1}$, and 2-hydroxybenzophenone: $490\,\text{L}\cdot\text{mol}^{-1}\cdot\text{cm}^{-1}$), both the depletion of the ester units (educt) as well as the yield of hydroxyketone (photo-Fries product) were assessed quantitatively.

A precise quantification from FT-IR spectra is only possible if the infrared absorbance coefficients of the hydroxyketones are determined for each individual compound. For a rough estimate the absorbance coefficients of a fully aromatic ester and its Fries rearrangement product were determined. For convenience, phenyl benzoate and 2-hydroxybenzophenone were chosen. In the case of phenyl benzoate, the absorbance coefficient A_{1736} of the ester carbonyl group is $700\,\text{L}\cdot\text{mol}^{-1}$. The ketone unit in 2-hydroxybenzophenone ($1630\,\text{cm}^{-1}$) absorbs with $A_{1630} = 490\ \text{L}\cdot\text{mol}^{-1}$ (both values obtained in dilute acetonitrile solutions). The ratio of the absorbance coefficients (ester : ketone) is 1.4 : 1 in this case.

An evaluation (as listed in Table 3.2) shows that the yield of the photo-Fries product is about 45 % for both polymers. This amount of *o*-hydroxyketone generated is high compared to other polymers based on aryl esters which undergo the photo-Fries rearrangement. A yield of 8 % was obtained for poly(naphthalene-1-yl 4-vinylbenzoate) as reported by Kern et al. [73]

The depletion of ester units can be approximated by an exponential fit (first order kinetics) which gives a "half period" $\tau = 1.17\,\text{J}\cdot\text{cm}^{-2}$ for PVP-**BZ** and $\tau = 0.94\,\text{J}\cdot\text{cm}^{-2}$ for PVP-**NA**. In this case, the term "half period" denotes

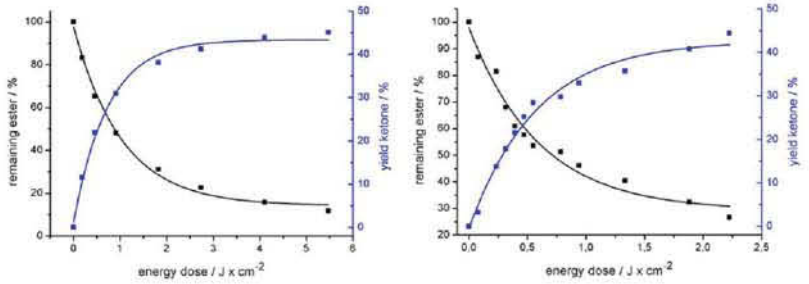

Figure 3.6: (a) Monitoring the photo-Fries rearrangement of PVP-**BZ** (irradiation wavelength: 254 nm). Depletion of the ester groups (black line) and generation of the *o*-hydroxyketone (blue line) determined by FT-IR spectroscopy (ester: 1730 cm^{-1}, ketone: 1630 cm^{-1}). An energy density of 2.2 $J.cm^{-2}$ is required to achieve a maximum ester conversion of 74 %. (b) Monitoring the photo-Fries rearrangement of PVP-**NA** (irradiation wavelength: 313 nm). Depletion of the ester groups (black line) and generation of the *o*-hydroxyketone (blue line) determined by FT-IR spectroscopy (ester: 1730 cm^{-1}, ketone: 1630 cm^{-1}). An energy density of 5.5 $J.cm^{-2}$ is required to achieve a maximum ester conversion of 88 %.

the energy density (in $J.cm^{-2}$) to degrade 50 % of the ester units under the selected irradiation conditions. The estimated progress of the photo-Fries reaction in PVP-**BZ** and PVP-**NA** is illustrated in Figure 3.6.

Spectroscopic ellipsometry was applied to determine the change in the refractive index upon UV irradiation. The Cauchy fits of the dispersion of the refractive indices of PVP-**BZ** and PVP-**NA** are shown in Figure 3.7. In these experiments, the duration of UV irradiation was adjusted to obtain a maximum yield of ketone. In both polymers, the refractive index showed a significant increase after illumination.

For PVP-**BZ** the refractive index increased by $\Delta n = 0.036$ at 600 nm and by $\Delta n = 0.027$ at 1200 nm, which is remarkably high for polymeric materials. Usually, refractive index variations in the range from 0.003 to 0.03 are already considered to be high. [74, 75]

For PVP-**NA**, refractive indices of $n = 1.656$ at 600 nm and $n = 1.618$ at 1200 nm were measured prior to illumination, respectively. After monochromatic irradiation with UV light of $\lambda = 313$ nm the refractive indices increased by $\Delta n = 0.011$ at 600 nm and by $\Delta n = 0.012$ at 1200 nm, respectively. These changes indicate large structural differences between the non-illuminated and the illuminated films as predicted for the proposed photo-Fries rearrangement.

Table 3.2: UV irradiation of the photoreactive polymers PVP-**BZ** and PVP-**NA**, conversion of the ester group and reaction yield of the photo-Fries product.

Compound	**Irradiation time**	**Energy density**	**Ester remaining**	***o*-Hydroxy-ketone generated**
	min	$J.cm^{-2}$	%	%
PVP-**BZ**	0	0	100	0
	2	0.18	83.23	11.54
	5	0.46	65.25	21.93
	10	0.91	48.08	30.88
	20	1.82	31.11	38.10
	30	2.74	22.63	41.27
	45	4.10	15.76	43.87
	60	5.47	11.72	45.02
PVP-**NA**	0	0	100	0
	30	0.08	86.86	3.21
	90	0.24	81.41	13.74
	120	0.31	67.95	17.86
	150	0.39	60.90	21.52
	180	0.47	57.69	25.18
	210	0.55	53.53	28.39
	240	0.78	51.28	29.76
	300	0.94	46.15	32.97
	360	1.33	40.38	35.71
	515	1.88	32.37	40.75
	720	2.22	26.60	44.41

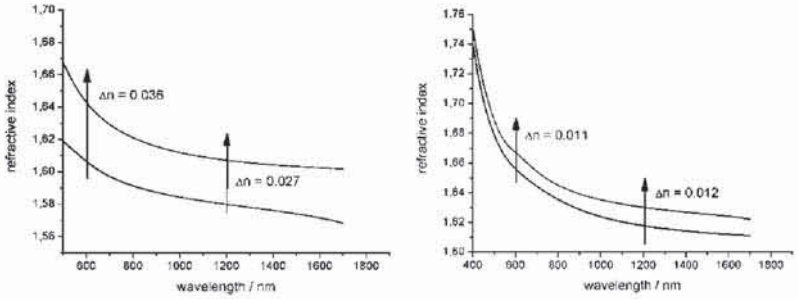

Figure 3.7: (a) Cauchy fits of the dispersion of the refractive index of a thin film of PVP-**BZ** prior to irradiation (black line), and after irradiation (red line) with an energy density of 5.47 J.cm^{-2} ($\lambda = 254$ nm) (b) Cauchy fits of the dispersion of the refractive index of a thin film of PVP-**NA** prior to irradiation (black line), and after irradiation (red line) with an energy density of 2.22 J.cm^{-2} ($\lambda = 313$ nm).

The large increase in the refractive index makes these polymers interesting for optical applications (such as waveguides and data storage devices).

Using photolithographic techniques both in PVP-**BZ** and PVP-**NA** refractive index patterns were generated. To create these patterns, thin films of PVP-**BZ** and PVP-**NA** were illuminated using a mask aligner system equipped with a suitable quartz-chromium mask (contact lithography). The features of the inscribed structures were visualized by optical microscopy using a phase contrast set-up. In Figure 3.8, phase contrast images of patterned films are depicted. In these images, areas with higher refractive indices appear dark, while areas with a lower refractive index appear bright. Both for PVP-**BZ** and PVP-**NA** the illuminated areas are clearly visible as dark features with higher refractive indices. Without any optimization, resolutions of 1 μm were achieved in this experiment.

In addition, the generation of *o*-hydroxyketones leads to an increase in the surface polarity of about 3 %. Table 3.3 summarizes the results from contact angle measurements before and after illumination of PVP-**BZ** and PVP-**NA**. The data on the surface tension γ and its dispersive (γ^D) and polar components (γ^P), as calculated by the Owens-Wendt method, are also presented.

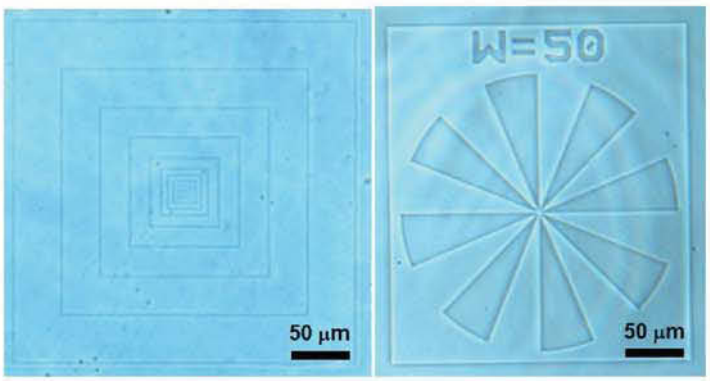

Figure 3.8: (a) Phase contrast image of PVP-**BZ** after UV patterning with a mask aligner (MJB4 from SUSS) using a 500 W HgXe lamp equipped with a filter for the range 235 nm - 265 nm (b) Phase contrast image of PVP-**NA** after UV patterning with a mask aligner (MJB4 from SUSS) using a 500 W HgXe lamp equipped with a filter for the range 270 nm - 320 nm.

Table 3.3: Contact angle (ϑ) and surface tension (γ = surface tension; γ^D = dispersive component; γ^P = polar component; surface polarity = 100 . $\frac{\gamma^P}{\gamma}$) for PVP-**BZ** and PVP-**NA** before and after illumination.

PVP-**BZ**						
yield ketone	ϑ H_2O	ϑ CH_2I_2	γ	γ^D	γ^P	surface polarity
%	deg	deg	$mN.m^{-1}$	$mN.m^{-1}$	$mN.m^{-1}$	%
0	84.4 (±1.3)	35.7 (±2.0)	43.60	41.70	1.90	4.4
33.9	81.9 (±1.9)	42.8 (±1.5)	41.35	38.19	3.16	7.6
PVP-**NA**						
yield ketone	ϑ H_2O	ϑ CH_2I_2	γ	γ^D	γ^P	surface polarity
%	deg	deg	$mN.m^{-1}$	$mN.m^{-1}$	$mN.m^{-1}$	%
0	86.3 (±1.5)	34.5 (±1.3)	43.64	42.25	1.39	3.2
13.4	82.9 (±0.9)	37.6 (±1.9)	43.20	40.81	2.40	5.6
38.7	82.2 (±2.7)	37.5 (±1.7)	43.43	40.82	2.61	6.0

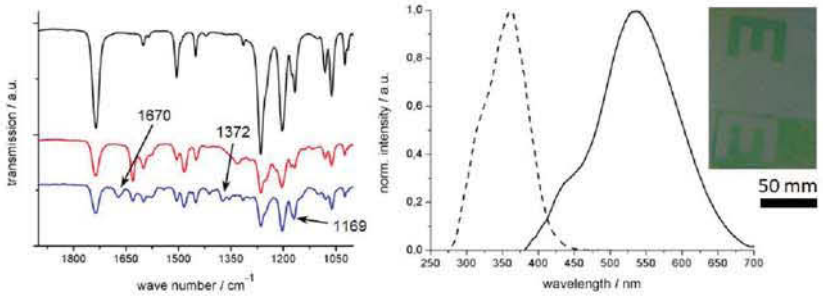

Figure 3.9: (a) FT-IR spectra of PVP-**BZ** prior to (black line) and after (red line) illumination, followed by post-treatment with dansyl chloride (blue line). $\lambda = 254\,\text{nm}$; radiant energy per unit area = $0.91\,\text{J}.\text{cm}^{-2}$ (b) Photoluminescence excitation (dashed line) and emission spectra (solid line) of phenyl 5-(dimethylamino)naphthalene-1-sulfonate dissolved in acetonitrile ($2.10^{-5}\,\text{mg/mL}$). Photograph of a film of PVP-**BZ** after patterned illumination and post-modification with dansyl chloride. (Photograph was taken during illumination with $\lambda = 366\,\text{nm}$).

3.2.2 Selective post-modification of PVP-BZ and PVP-NA

Another approach is the immobilization of fluorescent molecules in the irradiated areas of the polymeric film, using the reaction of the photogenerated hydroxyl groups with sulfonic acid chlorides. To demonstrate this, dansyl chloride was used. After UV illumination of a film of PVP-**BZ**, the sample was immersed in a solution of dansyl chloride and triethylamine in acetonitrile. The aromatic hydroxyl groups react readily with the sulfonic acid chloride to give the corresponding sulfonic acid ester. Figure 3.9a displays the FT-IR spectrum of an irradiated film of PVP-**BZ** after treatment with dansyl chloride. The changes in the spectrum are in accordance with the proposed reaction. The signal at $1631\,\text{cm}^{-1}$ (C=O stretching) is shifted to $1670\,\text{cm}^{-1}$. The appearance of new bands at $1372\,\text{cm}^{-1}$ and $1202\,\text{cm}^{-1}$ can be attributed to the asymmetric and symmetric SO_2 stretching vibrations. An additional band at $1169\,\text{cm}^{-1}$ is typical of the C-N stretching vibration of the R-N$(CH_3)_2$ groups which can be assigned to the corresponding unit in the dansyl chromophore.

The photoluminescence excitation and emission spectra of the dansyl fluorophore were measured using phenyl 5-(dimethylamino)naphthalene-1-sulfonate as a model compound. The dansyl fluorophore shows photoluminescence with the maximum of emission at $\lambda_{em} = 537\,\text{nm}$ and the maximum of excitation at $\lambda_{ex} = 361\,\text{nm}$, as illustrated in Figure 3.9b.

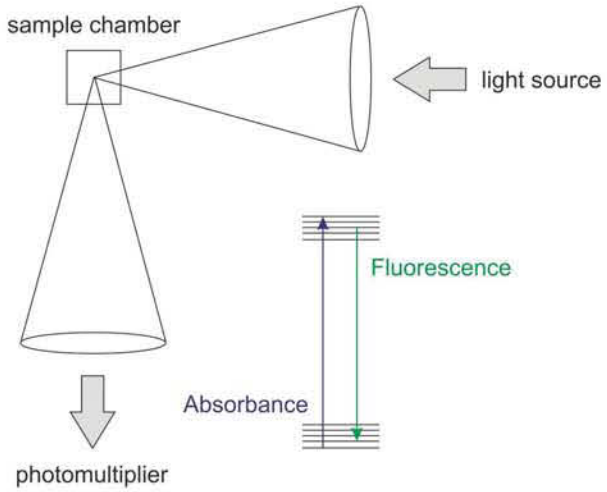

Figure 3.10: Simplified configuration of a fluorescence spectrophotometer.

As the excitation and the emission spectra overlap, one has to consider self-absorption effects. When light passes the sample, it has to cover a certain distance within the sample chamber, as illustrated in Figure 3.10. Some light covering a wavelength within the overlapping area is absorbed and subsequently emitted by the sample. Consequently, this influences the emission spectrum in quality and quantity.

Self-absorption effects decrease when the concentration of fluorescent molecules is reduced. In Figure 3.11 the results of a dilution series of phenyl 5-(dimethylamino)naphthalene-1-sulfonate in acetonitrile is shown. As the concentration is reduced, the absorbance is shifted towards lower wavelengths.

Fluorescent molecules bearing isothiocyanate groups can also be used for selective surface functionalization of the illuminated areas. For this purpose, a ruthenium based fluorescent dye was used. The photoluminescence excitation and emission spectra of this dye is shown in Figure 3.12b. An irradiated film was treated with a solution of $Ru(bpy)_2(phen\text{-}5\text{-}NCS)(PF_6)_2$ and triethylamine in acetonitrile. The aromatic hydroxyl groups react readily with the isothiocyanate groups to give the corresponding thiocarbamate derivative. Figure 3.12a displays the FT-IR spectrum of an irradiated film of PVP-**BZ** after treatment with $Ru(bpy)_2(phen\text{-}5\text{-}NCS)(PF_6)_2$. A new band evolves at about $1530\,cm^{-1}$ which can be assigned to the formation of the thiocarbamate group.

The immobilization of a Rhodamine B dye bearing NCS-groups is demon-

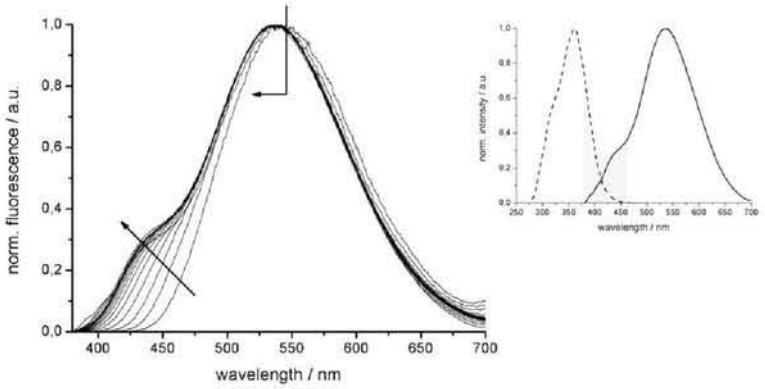

Figure 3.11: Dilution series of phenyl 5-(dimethylamino)naphthalene-1-sulfonate in acetonitrile from 2.5 mg/mL to $1.9.10^{-5}$ mg/mL; excitation wavelength $\lambda_{ex} = 360$ nm.

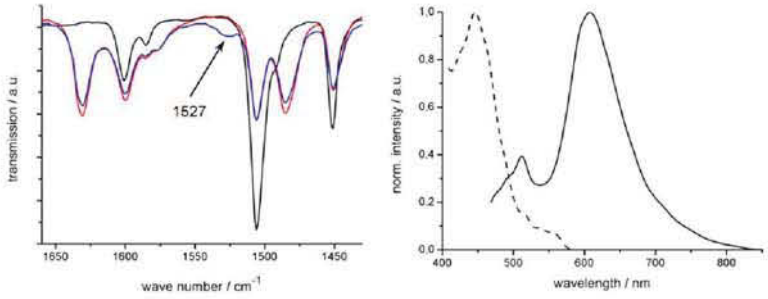

Figure 3.12: (a) FT-IR spectra of PVP-**BZ** before (black line) and after illumination (red line), followed by post-treatment with $Ru(bpy)_2(phen\text{-}5\text{-}NCS)(PF_6)_2$ (blue line). $\lambda = 254$ nm; radiant energy per unit area = $0.91\ J.cm^{-2}$ (b) Photoluminescence excitation (dashed line) and emission spectra (solid line) of $Ru(bpy)_2(phen\text{-}5\text{-}NCS)(PF_6)_2$ dissolved in acetonitrile ($1.56.10^{-2}$ mg/mL).

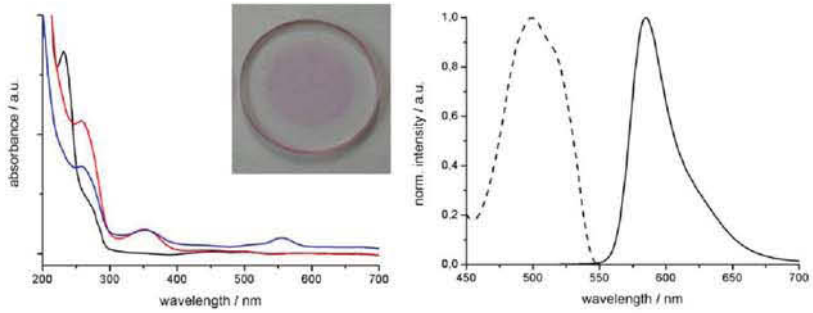

Figure 3.13: (a) UV/VIS spectra of PVP-**BZ** before (black line) and after illumination (red line), followed by post-treatment with Rhodamine B (blue line); $\lambda = 254\,\text{nm}$; radiant energy per unit area = $5.47\,\text{J.cm}^{-2}$ (b) Photoluminescence excitation (dashed line) and emission spectra (solid line) of Rhodamine B dissolved in ethanol ($1.56.10^{-2}$ mg/mL).

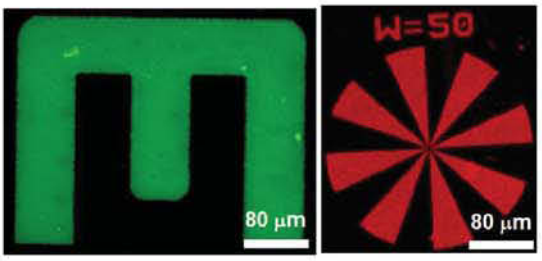

Figure 3.14: Optical micrograph of a thin film of PVP-**BZ** after structured illumination followed by post-treatment with dansyl chloride (left, $\lambda_{ex} = 405\,\text{nm}$) and $Ru(bpy)_2(phen\text{-}5\text{-}NCS)(PF_6)_2$ (right, $\lambda_{ex} = 488\,\text{nm}$). The images were recorded by confocal fluorescence microscopy using two different laser beams.

strated as well. Figure 3.13a displays the UV/VIS spectra of PVP-**BZ** before and after illumination followed by post-modification with Rhodamine B. As the modified areas of the polymeric film appear red, the immobilization reaction can be quantified by UV/VIS spectroscopy. An increase in absorbance between 585 nm and 600 nm can be observed, accompanied by the appearance of a new maximum localized at 555 nm.

In combination with lithographic techniques, these post-modification reactions can be used to prepare fluorescent patterns. The results of patterned modifications, using a mask aligner during the illumination step, are shown in Figure 3.21. The images were recorded by confocal fluorescence microscopy. Three-dimensional surface reconstructions are illustrated in Figure 3.15.

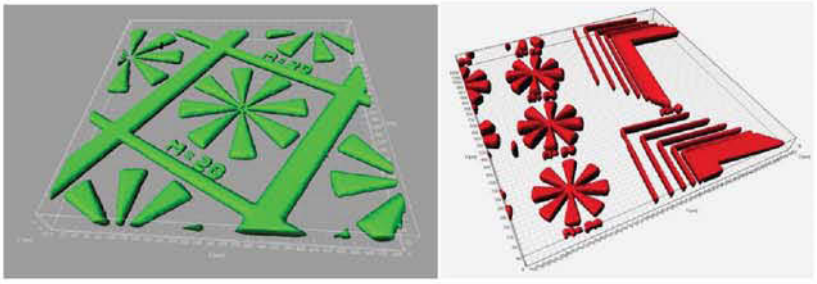

Figure 3.15: 3D-reconstructions of patterned films of PVP-**BZ** after post-modification reactions with dansyl chloride (left, $\lambda_{ex} = 405\,nm$) and $Ru(bpy)_2(phen\text{-}5\text{-}NCS)(PF_6)_2$ (right, $\lambda_{ex} = 488\,nm$).

The photo-generated *o*-hydroxyketones in PVP-**BZ** and PVP-**NA** can coordinate metal ions as reported previously. [76] For that reason irradiated films of PVP-**NA** were immersed in a solution of $FeCl_3$ in methanol for two hours, resulting in a slightly yellowish film.

The immobilization of Fe^{3+} ions was also proven by reaction with NH_4SCN in a solution of methanol, which led to the formation of a deeply red-colored iron(III) thiocyanate complex. The FT-IR spectrum (Figure 3.16) shows the typical strong bands of such a complex at $2075\,cm^{-1}$, which are assigned to the asymmetric N=C=S stretching vibration of inorganic thiocyanates.

Figure 3.17 shows the colored features obtained by patterned illumination of PVP-**NA** followed by a post-modification reaction using $FeCl_3$ and NH_4SCN, respectively.

3.2.3 Photoreaction of PVP-PY

PVP-**PY** could hardly be dissolved in common organic solvents such as dichloromethane or THF. Because of the poor solubility, PVP-**PY** showed also poor film forming properties when being spin-cast from a THF solution.

In a thin film of PVP-**PY** no photoreaction could be observed upon UV irradiation, as investigated by FT-IR spectroscopy (Figure 3.18a).

Figure 3.18b shows the UV/VIS spectrum of a cast film of PVP-**PY**. Absorption bands due to π-π^* transitions of pyrene were observed at 350 nm, 275 nm, 235 nm, and 220 nm. After illumination with UV light ($\lambda = 254$ nm), there was no change in absorbance.

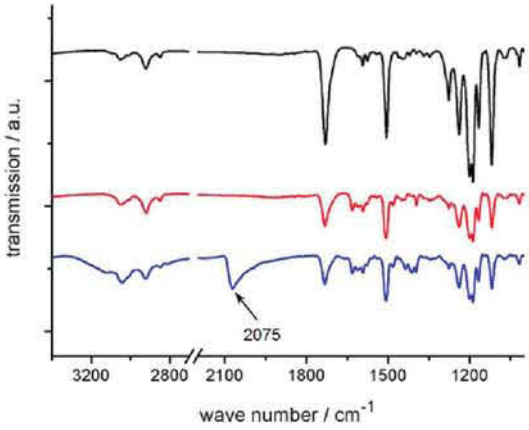

Figure 3.16: FT-IR spectra of PVP-**NA** before (black line) and after illumination (red line), followed by post-treatment with with Fe^{3+} and subsequently with NH_4SCN (blue line); $\lambda = 254\,nm$; radiant energy per unit area = $0.46\,J.cm^{-2}$.

Figure 3.17: Micrograph of a thin film of PVP-**NA** after patterned illumination and subsequent post-modification with $FeCl_3/NH_4SCN$.

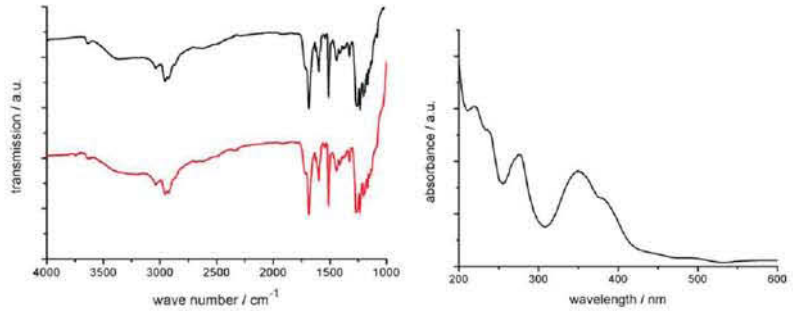

Figure 3.18: (a) FT-IR spectra of PVP-**PY** prior to (black line) and after illumination (red line). $\lambda = 254\,nm$; radiant energy per unit area = $5.47\,J.cm^{-2}$ (b) UV/VIS spectrum of PVP-**PY**.

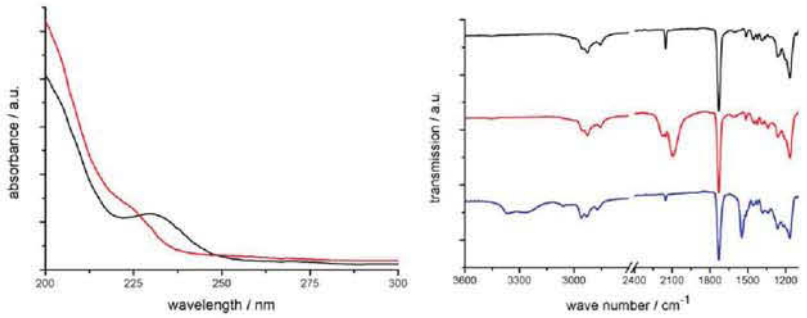

Figure 3.19: (a) UV/VIS spectra of PNOR-**SCN** prior to (black line) and after illumination (red line). $\lambda = 254\,\text{nm}$; radiant energy per unit area $= 0.63\,\text{J.cm}^{-2}$ (b) FT-IR spectra of PNOR-**SCN** prior to (black line) and after (red line) illumination, followed by post-treatment with propylamine (blue line). $\lambda = 254\,\text{nm}$; radiant energy per unit area $= 0.63\,\text{J.cm}^{-2}$

3.2.4 Photoreaction of PNOR-SCN

PNOR-**SCN** undergoes a photoisomerization from the thiocyanate to the corresponding isothiocyanate group. The benzyl thiocyanate group absorbs UV light up to 280 nm. Its photosensitivity is demonstrated by the infrared spectra taken before and after illumination with UV light ($\lambda = 254$ nm), see Figure 3.19 and Table 3.4.

The sharp peak of the vibration of the CN triple bond at $2153\,\text{cm}^{-1}$ decreases and two broad peaks emerge at $2180\,\text{cm}^{-1}$ and $2096\,\text{cm}^{-1}$ due to vibration of the cumulative double bonds of the NCS group. A small fraction of the thiocyanate groups is not converted. The thereby formed reactive isothiocyanate group easily forms a thiourea derivative when exposed to a solution of propylamine in acetonitrile for 3 min. The reaction is illustrated in Figure 3.20.

In the FT-IR spectrum, the two vibrational bands of the isothiocyanate unit completely vanish, and concomitantly the thiourea band at $1554\,\text{cm}^{-1}$ evolves. Unreacted SCN groups are detectable by the signal at $2153\,\text{cm}^{-1}$.

In addition, two broad bands at $3363\,\text{cm}^{-1}$ and $3260\,\text{cm}^{-1}$ (due to N-H stretching vibrations) appear. It becomes clear that FT-IR spectroscopy is an ideal tool to monitor both the progress of photoisomerization and the post-exposure reaction with amines. In a similar fashion, the addition reaction can be performed with fluorescent dyes bearing amino groups.

The SCN-NCS photoisomerization reaction was carried out in combination with lithographic techniques to give patterned polymer surfaces. The illumi-

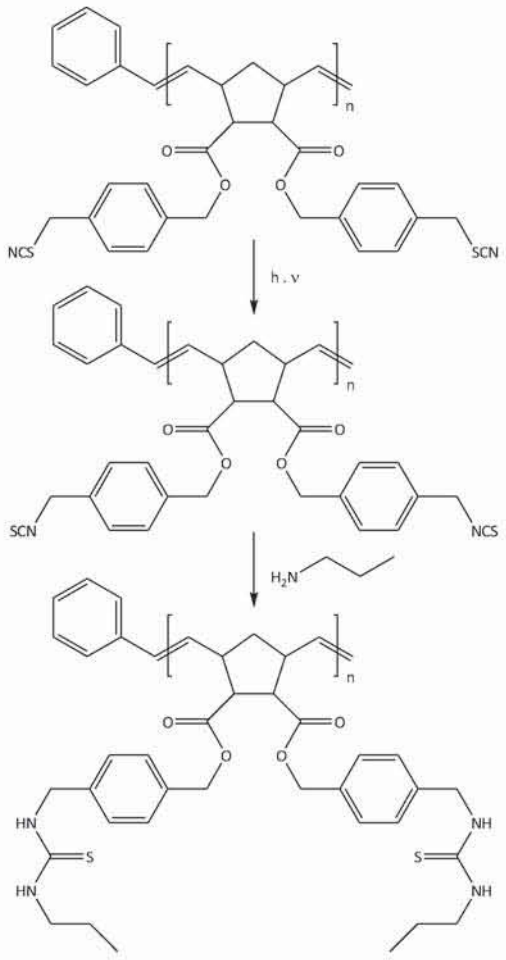

Figure 3.20: Photoreaction of PNOR-**SCN** and subsequent treatment with propyl amine to form a derivative of thiourea.

Table 3.4: Comparison of IR vibrations (values in cm^{-1}).

	PNOR-SCN	**Comments**
non-illuminated	2153	CN stretching vibration
illuminated	2180, 2096	asymmetric stretching vibration of NCS
+ **propylamine**	3363, 3260, 1554	N-H stretching vibration coupling between C=S and CN vibration

Figure 3.21: Optical micrograph of a thin film of PNOR-**SCN** after structured illumination (100 µm grating) followed by post-treatment with $Ru(bpy)_2(phen\text{-}5\text{-}NH_2)(PF_6)_2$ (CFM; $\lambda_{ex} = 488\,nm$).

nated areas are then capable of reacting with amines. For patterning of thin films of PNOR-**SCN**, a contact mask (100 µm grating) was placed onto the polymer film. After UV illumination the polymer layer was still optically transparent and no structural features were detectable by optical microscopy. After exposure to a solution of $Ru(bpy)_2(phen\text{-}5\text{-}NH_2)(PF_6)_2$, the structures of the mask pattern became visible under a confocal fluorescence microscope, see the image in Figure 3.21.

In this work, two dyes have been used for selective surface functionalization of thin films of PNOR-**SCN**: $Ru(bpy)_2(phen\text{-}5\text{-}NH_2)(PF_6)_2$, a red fluorescent dye, and 2-aminoacridone, a green fluorescent dye. The photoluminescence excitation and emission spectra of the respective compounds dissolved in acetonitrile are shown in Figure 3.22.

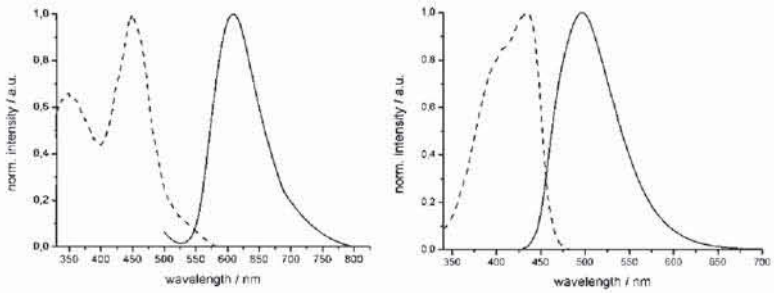

Figure 3.22: (a) Photoluminescence excitation (dashed line) and emission spectra (solid line) of $Ru(bpy)_2(phen\text{-}5\text{-}NH_2)(PF_6)_2$ dissolved in acetonitrile ($1.56.10^{-2}$ mg/mL). (b) Photoluminescence excitation (dashed line) and emission spectra (solid line) of 2-aminoacridone dissolved in acetonitrile ($1.56.10^{-2}$ mg/mL).

3.3 Dual-layer assembly

PVP-**BZ** absorbs light up to $\lambda \approx 300$ nm, which is typical of the phenyl chromophore with its π-π^* transition. The UV absorption of PVP-**NA** extends to 350 nm as expected for the naphthyl chromophore. Because of these different absorbance characteristics, a dual-layer assembly can be established.

A glass disk provides a non-photosensitive and semi-transparent interface between the two photoreactive layers.

Figure 3.23b shows the UV absorbance of the glass platelet compared to the two polymeric layers. The glass disk absorbs light up to $\lambda = 286$ nm and then starts to be light-transmissive for higher wavelengths. At $\lambda = 300$ nm about 89 % of the light can pass the interface while at $\lambda = 320$ nm the glass disk only absorbs about 1.5 % of the respective light.

While the naphthyl chromophores in PVP-**NA** absorb light above 300 nm, the phenyl rings in PVP-**BZ** do not absorb any light in this region. Since the glass interface is also transparent above 340 nm, a selective patterning of the PVP-**NA** layer from the top face with UV light > 340 nm can be performed. Moreover, in a second writing step the PVP-**BZ** layer can be patterned by UV light < 290 nm. Due to the fact that the glass interface absorbs UV light up to 320 nm the patterning of the PVP-**BZ** layer does not influence the PVP-**NA** layer. Consequently, each layer can be illuminated separately using two different light sources applied to the photosensitive films from the top of the assembly, as shown in Figure 3.23a.

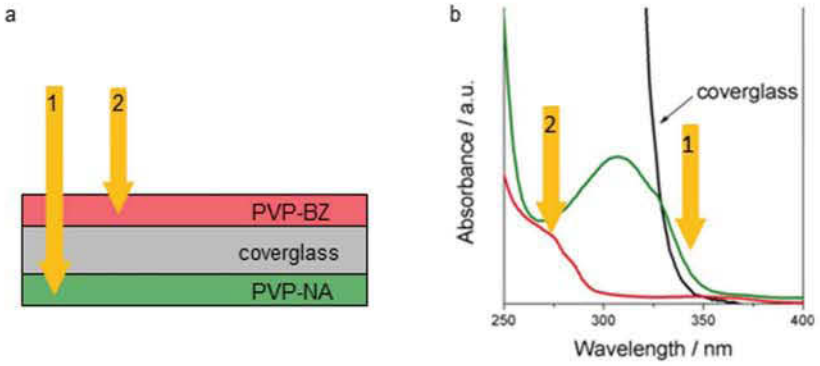

Figure 3.23: (a) Sketch of a dual-layer data storage device using two photosensitive polymeric layers (PVP-**BZ** on the top and PVP-**NA** on the bottom) and a thin glass substrate (about 100 µm) in between. (b) Comparison of the UV/VIS spectra of the polymeric films of PVP-**BZ** (red line) and PVP-**NA** (green line) with the UV absorbance of a coverglass (black line) for optical microscopy.

This approach of selective layer writing can be extended to a multilayer assembly using different photosensitive polymers and filter layers. The utilization of absorption differences in such polymer layers combined with appropriate filter layers in multilayer assemblies provides the possibility of selective refractive index patterning in different polymer layers without the demand of a two-photon absorption process.

In general, confocal reflection-type systems are used for recording and reading out data in such type of multilayer recording devices. Moreover, sandwich structures of polymer films and non-photosensitive layers, i.e., glass slides improves the readout quality due to the high optical contrast of these materials already mentioned by Ishikawa et al. [67]

Considering the huge number of various possible glass types providing absorption onsets between 200 - 400 nm and the versatility of organic chemistry which allows the synthesis of polymers providing different absorption behaviours it is conceivable to create data storage devices with several recording layers. This makes these UV-reactive polymeric materials interesting candidates for application in novel bitwise volumetric data storage devices.

Using a mask aligner in combination with a contact mask, patterns can be generated on each polymeric layer. In combination with the $FeCl_3/NH_4SCN$ post-modification it is possible to show both layers in transmission mode as depicted in Figure 3.24. The illumination was performed using a contact mask

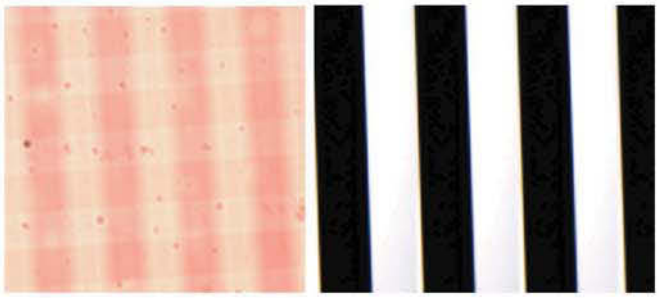

Figure 3.24: Dual-layer patterning of PVP-**BZ** and PVP-**NA** followed by $FeCl_3$/ NH_4SCN post-modification (left); 100 µm grating used as a contact mask for the photolithographic patterning (right).

(lattice spacing: 100 µm) which was rotated by 90° after illuminating the bottom layer.

For a better visibility of the obtained refractive index patterns the previously mentioned staining process with reactive fluorescent dyes (vide infra) has been applied to this dual layer approach. Therefore, each layer of the assembly has been immersed in a solution of dansyl chloride and $Ru(bpy)_2$(phen-5-NCS)$(PF_6)_2$ in acetonitrile upon the patterning procedure, respectively.

Consequently, both fluorescent dyes could be immobilized in the irradiated areas of the polymeric layers. Figure 3.29 shows the three-dimensional reconstruction of an image recorded by confocal fluorescence microscopy. In the top layer, consisting of an patterned film of PVP-**BZ**, $Ru(bpy)_2$(phen-5-NCS)$(PF_6)_2$ was immobilized which shows red fluorescence when excited by a 488 nm laser. The illuminated areas of the bottom layer (PVP-**NA**) were modified with dansyl chloride and therefore excitation with a 405 nm laser beam leads to the emission of green light. The lattice spacing of the contact mask was 100 µm.

This dual-layer assembly can be adapted to optical applications such as multiple layer optical data storage. Photolithographic techniques in combination with the immobilization of fluorescent dyes within the illuminated areas of the polymeric matrix can be used to improve the signal-to-noise ratio of such devices. This principle has already been realized in commercially available storage mediums known under the term fluorescent multi-layer storage (FMS). (10)

Using two different light sources allows each layer to be patterned separately, which makes these types of materials interesting for dual-layer optical data storage applications. Confocal reflection-type systems can be used for

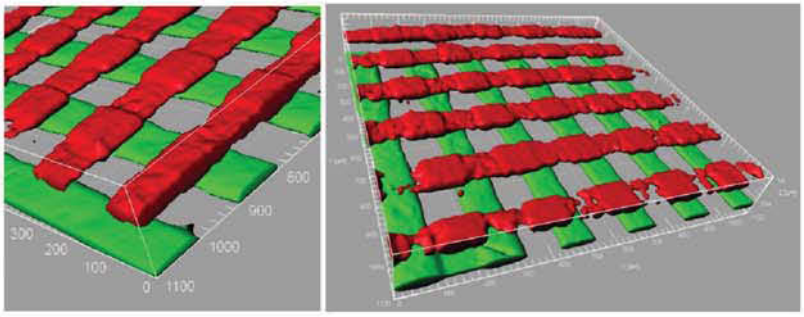

Figure 3.25: Three-dimensional reconstruction of the patterned films of PVP-**BZ** and PVP-**NA** within the dual-layer assembly. The original signal was recorded by confocal fluorescence microscopy after post-modification with fluorescent dyes. The 3D-image was created with the software Imaris 6.4.2 (Bitplane, Zurich, Switzerland)

recording and reading data, and by the use of color filters interference signals can be minimized. Since the data marks produce incoherent fluorescence when illuminated by the readout laser beam, there are no missing Fourier cones as known in refractive index change materials. The basic design of such a device is illustrated in Figure 3.26.

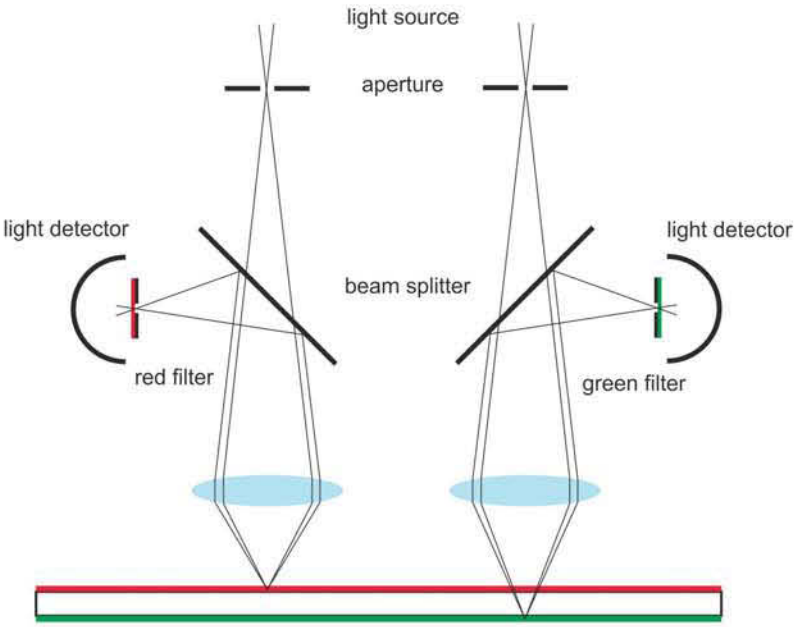

Figure 3.26: Basic design of a confocal reflection-type system for recording and reading data from a fluorescent dual-layer data storage device.

3.4 Investigation of the OLED

Polymers with large energy bandgaps that emit blue light efficiently are of special interest because these materials are desirable either as blue light sources in full color displays, or as host materials for generating other colors through energy transfer to lower energy fluorophores. [77, 78]

Because of their high photoluminescence and electroluminescence efficiencies, good thermal stabilities, solubility, and film-forming capabilities, polyfluorenes (PFOs) are very promising candidates for preparing blue light emitting materials. [79, 80] Facile methods for functionalizing the C_9 position of the fluorene unit also offer the possibility of tuning the opto-electronic properties of PFOs through macromolecular engineering. [81, 82, 83, 84, 85]

In conjugated polymers, Förster resonance energy transfer (FRET) between two chromophore segments that have different energies is fast and efficient, and it shifts the emission to longer wavelengths. [86, 87] Common ways of applying dye molecules in electroluminescent devices are blending with a conjugated polymer matrix and physical vapor deposition of the dye onto a layer of a conjugated

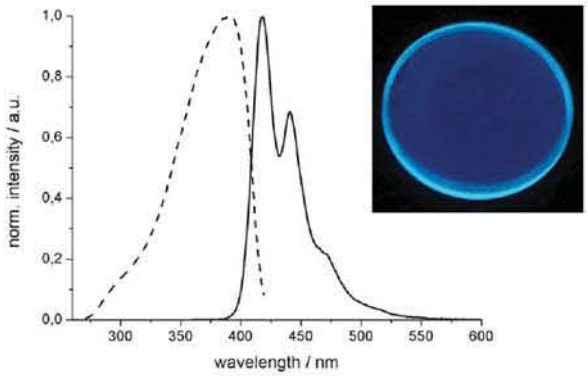

Figure 3.27: Photoluminescence excitation (dashed line) and emission spectra (solid line) of Poly(9,9-dioctylfluorenyl-2,7-diyl) end capped with 2,5-diphenyl-1,2,4-oxadiazole (ADS429BE) dissolved in chloroform ($1.6.10^{-2}$ mg/mL). Macroscopic image of film on CaF_2 plate was taken during illumination with $\lambda = 366$ nm.

polymer. In addition, copolymers have been prepared that contain monomer units such as fluorene and a dye molecule in the main chain without interruption of the conjugation [88, 89, 90] as well as without the continuation of the conjugation in the backbone. [91]

In this work, a dioctyl-modified PFO derivative end capped with 2,5-diphenyl-1,2,4-oxadiazole was used. Its photoluminescence excitation and emission spectra are illustrated in Figure 3.27. The electroluminescent polymer itself was not modified, but physically mixed with the photoreactive PNOR-**SCN**. Blends of 40 % PFO and 60 % PNOR-**SCN** were prepared and films were spin-cast from 10 mg/mL chloroform solutions onto the PEDOT:PSS layer as described in section 5.6.

Due to the thiocyanate – isothiocyanate conversion under exposure to UV light, amino-functionalized acceptor molecules can be immobilized in the illuminated areas, as demonstrated by FT-IR spectroscopy as well as confocal fluorescence microscopy in section 3.2.4.

In order to achieve a sufficient energy transfer from the PFO derivative to the fluorescent dye, good spectral overlap is required. The photoluminescence emission spectrum of the electroluminescent polymer must overlap the absorption spectrum (photoluminescence excitation) of the respective dye. In the case of $Ru(bpy)_2(phen\text{-}5\text{-}NH_2)(PF_6)_2$, a sufficient spectral overlap can be obtained, as shown in Figure 3.22. However, by the choice of 2-aminoacridone no sufficient

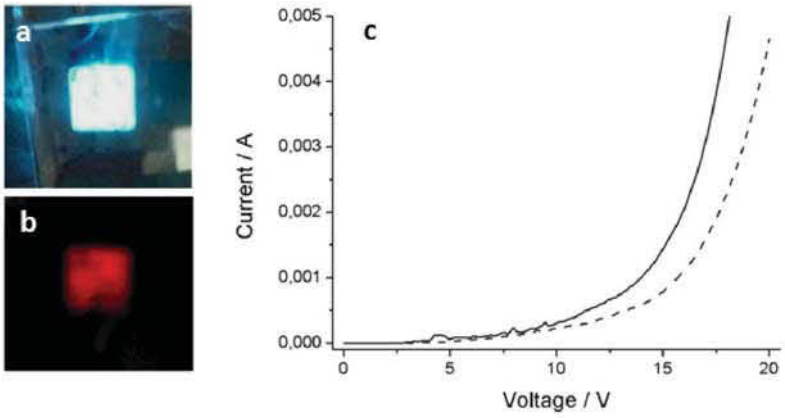

Figure 3.28: (a) Photograph of an OLED using a blend of polyfluorene and PNOR-**SCN** as emitting layer. (b) Photograph of the modified OLED (after UV-illumination and post-treatment with $Ru(bpy)_2(phen\text{-}5\text{-}NH_2)(PF_6)_2$). (c) Current-voltage characteristics of the modified (dashed line) and the non-modified (solid line) OLED.

energy transfer could be achieved.

Without illumination and post-modification the polymer blend shows bright blue electroluminescence as depicted in Figure 3.28a. In contrast, when the film is illuminated using UV light ($\lambda = 254\,nm$) and exposed to a solution of $Ru(bpy)_2(phen\text{-}5\text{-}NH_2)(PF_6)_2$ in acetonitrile, the blue emission completely disappears and the device shows bright red electroluminescence as it can be seen in Figure 3.28b.

The current-voltage (I-U) characteristics of these OLEDs in Figure 3.28c show p-type character revealing a significant higher onset voltage for the devices in which the Ru(II) complex was immobilized.

In reality, one can observe the emission of the host molecule, the guest molecule, or a combination of both, depending on the efficiency of the energy transfer processes. The higher the efficiency of the energy transfer, the brighter the red emission color gets until no blue color is observable.

Considering the critical quenching radius, as mentioned in section 2.4.4, swelling of the polymeric film in the acetonitrile solution is required, as the dye molecules have to diffuse into the emissive layer. Only deficient energy transfer would occur unless uniform mixing is achieved.

Moreover, the energy transfer from the blue-emitting donor polymer to the

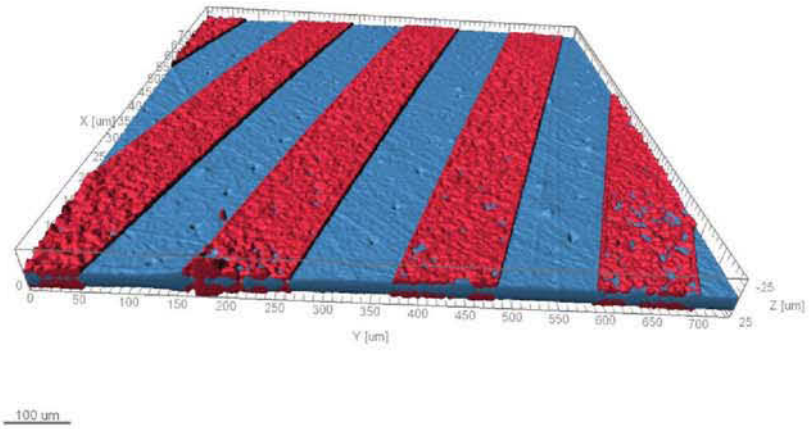

Figure 3.29: Three-dimensional reconstruction of a patterned film of PNOR-**SCN**/PFO with a PFO content of 1 %. The original signal was recorded by confocal fluorescence microscopy after patterned irradiation followed by post-modification with a fluorescent dye. The 3D-image was created with the software Imaris 6.4.2 (Bitplane, Zurich, Switzerland)

attached red-emitting host material is investigated by means of confocal fluorescence microscopy.

Thin films of PNOR-**SCN**/PFO blend on CaF_2-plates were spin-cast from chloroform solution with a PFO content of 1 %. The films were patterned by using a mask aligner equipped with a filter transmissive for the wavelength range from 235 nm to 265 nm. Four cycles of 5 min illumination time and a 30 s cooling period after each cycle were applied to the polymeric films. The patterned films were immersed in a solution of $Ru(bpy)_2(phen\text{-}5\text{-}NH_2)(PF_6)_2$, a red fluorescent dye, in acetonitrile for two hours.

Figure 3.29 shows the three-dimensional reconstruction of such a film. Both the irradiated and the non-irradiated areas were excited using a 405 nm laser. The non-illuminated areas show blue fluorescence which is caused by the PFO derivative. The illuminated areas appear in a deeply red color due to the energy transfer from the donor, PFO, to the attached red-emitting fluorescent dye.

Chapter 4

Summary

In this contribution, the photo-Fries rearrangement in combination with post-exposure modification reactions for the patterning and functionalization of polymeric films were investigated. The photo-Fries reaction generates reactive hydroxyketone groups, which can be employed for a selective modification of the irradiated areas. Post-treatment reactions using fluorescent molecules that can be easily attached to the polymeric surface have been shown. In combination with lithographic processes fluorescence patterns with bright luminescence were obtained.

Both, the photoreaction and the selective modifications can be monitored by FT-IR and UV/VIS spectroscopy. Quantitative FT-IR spectroscopy proved to be an appropriate tool because the functional group in the educt (i.e., the ester unit) and the functional group in the expected photo-Fries product (i.e., hydroxyketone) display well-resolved signals in the infrared spectrum as depicted in Figure 4.1.

Two polymers, poly(4-vinylphenyl benzoate) (PVP-**BZ**) and poly(4-vinylphenyl 1-naphthoate) (PVP-**NA**) were synthesized via polymer analogous esterification of commercially available poly(4-vinyl phenol). Upon UV irradiation a significant change in the refractive index by $\Delta n_{600} = +0.036$ for PVP-**BZ** and by $\Delta n_{600} = +0.011$ for PVP-**NA** was observed. The large increase in the refractive index makes these polymers interesting for optical applications (such as waveguides and data storage devices).

Using photolithographic techniques both in PVP-**BZ** and PVP-**NA** refractive index patterns were generated. To create these patterns, thin films of PVP-**BZ** and PVP-**NA** were illuminated by using a mask aligner system and

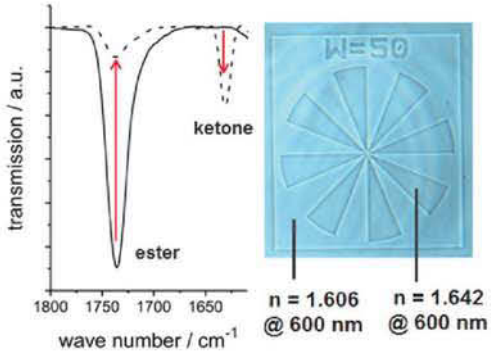

Figure 4.1: Change in FT-IR spectrum (left) and a phase contrast image of PVP-**NA** after UV patterning with a mask aligner (right).

a quartz-chromium mask (contact lithography). The features of the inscribed structures were visualized by optical microscopy using a phase contrast set-up, as shown in Figure 4.1.

In combination with post-modification reactions, fluorescent patterns can be obtained. Consequently, these polymers combine the advantages of both refractive index materials and fluorescent materials which make them interesting candidates for optical data storage devices.

Due to the fact that both synthesized polymers exhibit different light absorption characteristics novel approaches of bitwise volumetric recording could be demonstrated. Using a coverglass as optical filter between the polymeric films it was possible to achieve a selective patterning of each layer via UV light of different wavelengths without the demand of two-photon excitation. The generated patterns could be visualized by CFM, as shown in Figure 4.2.

In addition, (±)endo,exo-bicyclo[2.2.1]hept-5-ene-2,3-dicarboxylic-bis-(4-thiocyanatomethyl)benzylester (NOR-**SCN**) was synthesized and polymerized via ring-opening metathesis polymerization (ROMP). The attached thiocyanate groups undergo a conversion to isothiocyanate groups upon UV irradiation.

Fluorescent molecules bearing amino groups can be easily attached to the polymeric surface under the formation of thiourea derivatives, and in combination with lithographic processes fluorescence patterns with bright luminescence are obtained. Both, the photoreaction and the post-treatment can be easily monitored by FT-IR and UV/VIS spectroscopy.

This provides the opportunity of selective surface functionalization by phys-

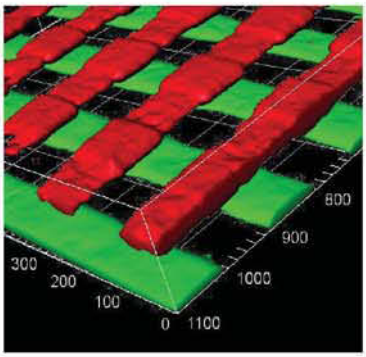

Figure 4.2: A three-dimensional reconstruction of the stained dual layer assembly. The original signal was recorded by confocal fluorescence microscopy after post-modification with fluorescent dyes.

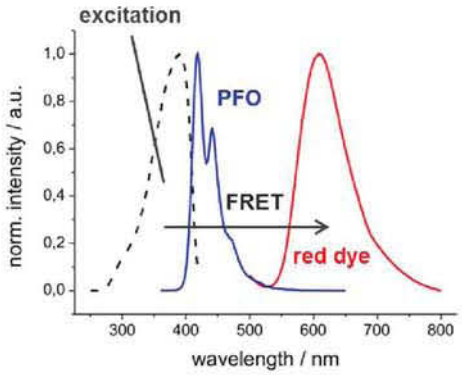

Figure 4.3: Color-tuning by Förster resonance energy transfer (FRET) from the PFO donor to the dye acceptor.

ical mixing with a fluorene-based electroluminescent polymer followed by photolithographic patterning and post-modification with a fluorescent dye. Due to Förster resonance energy transfer (FRET), tuning of the emission color can be achieved.

In order to achieve a sufficient energy transfer from the PFO derivative to the fluorescent dye, good spectral overlap is required. The photoluminescence emission spectrum of the electroluminescent polymer must overlap the absorption spectrum (photoluminescence excitation) of the respective dye. In the case of $Ru(bpy)_2(phen\text{-}5\text{-}NH_2)(PF_6)_2$, the dye meets the specified requirements, as demonstrated in Figure 4.3.

Chapter 5

Experimental

5.1 Equipment

5.1.1 Chemicals

All chemicals were purchased from commercial sources and used without further purification (Figure 5.1). All experiments were carried out under nitrogen atmosphere using Schlenk techniques or a glovebox, respectively.

5.1.2 Instruments and methods

Thin layer chromatography (TLC)

"Alugram® SIL G/UV" plates from Machery-Nagel were used as stationary phase in thin layer chromatography. The mobile phase was cyclohexane and ethyl acetate in various ratios. A low-pressure mercury lamp at 254 nm was used for detection.

Column chromatography

Silica 60A from Fisher Scientific with a particle size of 60 - 200 µm was used as a stationary phase in column chromatography. Various mixtures of cyclohexane and ethyl acetate were used as eluents.

Table 5.1: List of chemicals.

substance	producer	grade
acetonitrile	Fisher Scientific	99.99 %
2-aminoacridone	Fluka	purum, $\geq$ 98.0 %
ammoniumthiocyanate	Fluka	purum p.a. $\geq$ 98.5 %
Baytron P (PEDOT:PSS)	Bayer	n/a
benzoyl chloride	Sigma Aldrich	99 %
chloroform-D	Acros	99.8 atom-% D, stabilized
(4-chloromethyl)benzyl alcohol	Aldrich	99 %
cyclohexane	Roth	$\geq$ 99.5 %
dansyl chloride	Fluka	$\geq$ 99.0 %
dichloromethane	Sigma Aldrich	anhydrous, $\geq$ 99.8 %
DMSO	Merck	p.a.
(±)endo,exo-bicyclo[2.2.1]hept-5-ene-2,3-dicarbonyl dichloride	Aldrich	99 %
ethyl acetate	J.T. Baker	$\geq$ 99.5 %
ethyl vinyl ether	Aldrich	99 %
(H2IMes)(PCy3)(Cl)2Ru=CHPh	Aldrich	n/a
hydrochloric acid	Roth	37 %
iron(III)chloride	Sigma Aldrich	$\geq$ 97 %
isopropyl alcohol	Acros	99.8 %
methanol	Fluka	p.a.
1-naphthoyl chloride	Aldrich	97 %
phenol	Fluka	purum, $\geq$ 99 %
PFO (ADS429BE)	ADS	n/a
poly(4-vinylphenol) Mw = 11 000	Aldrich	n/a
propylamine	Fluka	purum, $\geq$ 99.0 %
1-pyrenecarboxylic acid	Aldrich	97 %
pyridine	Sigma Aldrich	anhydrous, $\geq$ 99.8 %
Rhodamine B isothiocyanate	Aldrich	mixed isomers
$Ru(bpy)_2(phen\text{-}5\text{-}NH_2)(PF_6)_2$	Sigma	n/a
$Ru(bpy)_2(phen\text{-}5\text{-}NCS)(PF_6)_2$	Sigma	n/a
sodium hydrogencarbonate	Fluka	$\geq$ 99.0 %
sodium hydroxide	Fluka	purum, $\geq$ 97 %
sodium sulfate	Merck	anhydrous, p.a.
thionyl chloride	Fluka	purum, $\geq$ 99.0 %
THF	Sigma Aldrich	puriss. stabilized, p.a.
toluene	Riedel-de-Haën	p.a.
triethylamine	Sigma Aldrich	99 %

Size exclusion chromatography (SEC)

The weight and number average molecular weights (M_w and M_n) as well as the polydispersity index (PDI) were determined by gel permeation chromatography (GPC) with tetrahydrofuran (THF) as solvent using the following setup: Micro-volume double pistol pump, flow rate 1 mL.min^{-1}, separation columns from VARIAN, particle size 5 µm, combined refractive index viscosity detector. Polystyrene standards from POLYMER LABS were used for calibration.

FT-IR spectroscopy

FT-IR spectra were recorded with a PERKIN ELMER "Spectrum One" instrument (spectral range between 4000 and 450 cm^{-1}, resolution 1 cm^{-1}). All FT-IR spectra were recorded in transmission mode.

UV/VIS spectroscopy

UV/VIS spectra were measured with a VARIAN Cary 50 UV/VIS spectrophotometer. All UV/VIS spectra were taken in the absorbance mode.

NMR spectroscopy

^{1}H-NMR and ^{13}C-NMR spectra were recorded with a VARIAN 400-MR spectrometer operating at 399.66 MHz and 100.5 MHz, respectively. A relaxation delay of 10 s and 45° pulse were used for acquisition of the ^{1}H-NMR spectra. Solvent residual peaks were used for referencing the NMR spectra to the corresponding values given in literature. [92]

Differential Scanning Calorimetry (DSC)

The thermal characterization was carried out on a PERKIN-ELMER Pyris Diamond differential scanning calorimeter which is equipped with a PERKIN-ELMER CCA7 cooling system (liquid nitrogen circulation). The measurements were performed under a nitrogen flow of 20 mL/min and at heating rates of 10 °C/min and 20 °C/min, respectively. Glass transition temperatures (T_g) were read as the midpoint of change in heat capacity.

Determination of absorbance coefficients

For quantitative analysis of the photo-Fries reaction, the infrared absorbance coefficients of model compounds, phenyl benzoate (educt) and 2-hydroxybenzo-

phenone (product) were determined. Solutions that contained equimolar amounts of educt and product in acetonitrile (between 1.0 and 10.0 mmol.L^{-1}) were measured in a liquid cell with KBr windows. The optical path length was 117 µm as determined with a precision gauge. The signal heights of the ester carbonyl band of phenyl benzoate (1736 cm^{-1}) and the ketone carbonyl band of 2-hydroxybenzophenone (1630 cm^{-1}) were evaluated using a tangent fit method. The absorbance values showed a linear dependence on the concentration of the respective model compound. From linear regression the absorbance coefficients were calculated.

phenyl benzoate: 700 $L.mol^{-1}.cm^{-1}$

2-hydroxybenzophenone: 490 $L.mol^{-1}.cm^{-1}$

Illumination

UV irradiation experiments were carried out using a medium pressure Hg lamp (100 W, from NEWPORT, model 66990) equipped with a filter for 313 nm, and an ozone free low pressure Hg lamp (HEREAUS Noblelight, 254 nm). In these experiments the light intensity (integrated power density) at the sample surface was measured with a spectroradiometer (SOLATELL, Sola Scope 2000TM, spectral range from 230 to 470 nm). The light intensities were 0.0436 $mW.cm^{-2}$ for 313 nm (medium pressure Hg lamp), and 2.1 $mW.cm^{-2}$ for 254 nm (low pressure Hg lamp). All UV illuminations were carried out under inert gas atmosphere (N_2).

Ellipsometric measurements

Ellipsometric measurements were performed at the Institute for Surface Technologies and Photonics at JOHANNEUM RESEARCH in Weiz, Austria. For sample preparation, solutions of the corresponding polymers (15 mg/mL in dichloromethane) were spin-cast onto silicon wafers. A WOOLLAM VASE spectroscopic ellipsometer was used (xenon short arc lamp, wavelength range 240 - 1100 nm, spectral bandwidth 5 nm). The detector system consists of crystal polarizers and silicon diodes (rotating composition) with an additional phase compensator (auto-retarder) to compensate phase differences which occur between 0° and 180°.

Phase differences in an area between 0° and 360° can be measured. The implemented software uses the Levenberg-Marquardt fit algorithm. From ellipsometric data both the film thickness and the dispersion of the refractive index (Cauchy fit) were obtained.

Optical microscopy

The patterned polymeric films were investigated using an OLYMPUS BX51 light microscope (OLYMPUS, Hamburg, Germany) either in the reflection or in the transmission mode. For visualizing the change in the refractive index, the reflection mode combined with a phase contrast accessory was used which enhances contrasts of transparent and colorless objects by influencing the optical path of light.

Confocal fluorescence microscopy

Confocal microscopy was performed with a LEICA TCS SPE confocal microscope (LEICA Microsystems, Wetzlar, Germany). The dansyl fluorophore was excited with a 405 nm laser beam and the light emitted in the range 460 - 540 nm was detected. $Ru(bpy)_2(phen\text{-}5\text{-}NCS)(PF_6)_2$ was excited with a 488 nm laser beam and the light emitted in the range 575 - 635 nm was detected.

Photomultiplier gain and offset were individually optimized for every channel and every field of view, in order to reduce the noise. Confocal stacks were acquired with a LEICA 10x dry APO objective (*NA*: 0.30) by applying a Z-step of 4 µm. Three-dimensional reconstructions were created with the software Imaris 6.4.2 (BITPLANE, Zurich, Switzerland).

Contact angle measurements

The surface tension γ of the sample surfaces was determined by measuring the contact angle with a Drop Shape Analysis System DSA100 (KRÜSS GmbH, Hamburg, Germany) using water and diiodomethane as test liquids (drop volume 3 µL, drop rate 195.1 µL/min). The contact angles were obtained by means of the sessile drop method and they were measured within 2 s. The mean values of twelve individual measurements were calculated, the reproducibility was within 2°. Based on the Owens-Wendt method, the surface tension γ as well as the dispersive and polar components (γ^D and γ^P) were evaluated.

5.2 Synthesis

5.2.1 Synthesis of (4-thiocyanatomethyl)benzyl alcohol

1.0 g (6.39 mmol) of (4-chloromethyl)benzyl alcohol dissolved in 10 mL THF was added to a solution of 0.97 g (12.78 mmol) ammonium thiocyanate in 5 mL THF and the mixture was refluxed for 20 h. The solvent was evaporated and the residue was dissolved in dichloromethane. The remaining precipitate was filtered off, and the solution was evaporated in vacuo. The residual crude product was purified by column chromatography (50 g silica gel, cyclohexane/ethyl acetate 5/1).

Yield: 1.14 g (99 %) of an oily liquid

^{1}H-NMR (400 MHz, 20 °C, $CDCl_3$) δ 7.36 (dd, 4H, Ph), 4.69 (s, 2H, -CH_2-OH), 4.15 (s, 2H, -CH_2-SCN)

^{13}C-NMR (100 MHz, 20 °C, $CDCl_3$) δ 141.9 (1C, Ph^4), 133.7 (1C, Ph^1), 129.3 (2C, $Ph^{3,5}$), 127.7 (2C, $Ph^{2,6}$), 112.1 (1C, SCN), 64.8 (1C, -CH_2-OH), 38.2 (1C, -CH_2-SCN)

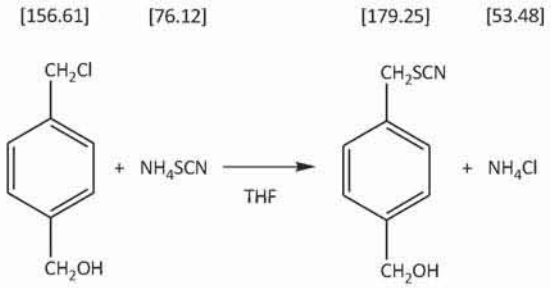

Figure 5.1: Synthesis of (4-thiocyanatomethyl)benzyl alcohol.

5.2.2 Synthesis of (±)endo,exo-bicyclo[2.2.1]hept-5-ene-2,3-dicarboxylic-bis-(4-thiocyanatomethyl)benzyl ester

To a solution of 0.62 g (3.46 mmol) (4-thiocyanatomethyl)benzyl alcohol and 0.72 mL (5.19 mmol) triethylamine in 5 mL dichloromethane 0.25 mL (±)endo,exo-bicyclo[2.2.1]hept-5-ene-2,3-dicarbonyl dichloride dissolved in 5 mL dichloromethane were added dropwise. After refluxing for 60 h the obtained white precipitate was filtered off and the solution was extracted with HCl (5 %) and subsequently with saturated $NaHCO_3$. The organic layer was separated, dried over Na_2SO_4 and evaporated in vacuo. The residual crude product was purified by column chromatography (50 g silicagel, cyclohexane / ethyl acetate 2/1).

Yield: 307 mg (34.1 %) of a white powder

^{1}H-NMR (400 MHz, 20 °C, $CDCl_3$) δ 7.36 (d, 8H, Ph), 6.27 (dd, 1H, Nb^6), 6.00 (dd, 1H, Nb^5), 5.2 - 5.1 (m, 1H, -O-CH_2-), 4.16 (s, 4H, -CH_2-SCN), 3.46 (t, 1H, Nb^3), 3.30 (s, 1H, Nb^4), 3.16 (s, 1H, Nb^1), 2.78 (m, 1H, Nb^2), 1.62 - 1.47 (m, 2H, Nb^7)

^{13}C-NMR (100 MHz, 20 °C, $CDCl_3$) δ 174.2 - 173.0 (2C, -C=O), 137.8 (1C, Nb^6), 137.0 - 136.9 (2C, $Ph^{4,4'}$), 135.2 (1C, Nb^5), 134.5 - 134.5 (4C, $Ph^{1,1'}$), 129.4 - 129.3 (4C, $Ph^{3,3',5,5'}$), 128.8 (2C, $Ph^{2,2',6,6'}$), 112.0 (2C, -SCN), 66.2 - 65.9 (2C, -O-CH_2), 48.2 (1C, Nb^3), 47.9 (1C, Nb^1), 47.5 (1C, Nb^7), 47.4 (1C, Nb^2), 45.9 (1C, Nb^4), 38.1 (2C, -CH_2-SCN)

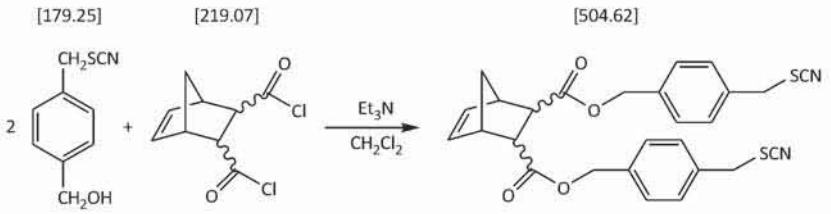

Figure 5.2: Synthesis of (±)endo,exo-bicyclo[2.2.1]hept-5-ene-2,3-dicarboxylic-bis-(4-thiocyanatomethyl)benzyl ester.

5.2.3 Synthesis of Grubbs catalyst 3rd generation [93, 94]

To a solution of $(H_2IMes)(PCy_3)(Cl)_2Ru{=}CHPh$ (Grubbs catalyst 2nd generation; 100 mg; 0.1178 mmol) in 5 mL toluene 1 mL pyridine (0.0124 mmol) was added dropwise while stirring constantly, which lead to a color change from purple to green. After 3 hours the catalyst was precipitated in 40 mL cold *n*-heptane. Finally, it was filtered off, washed with *n*-heptane and dried in vacuo.

Yield: 57.7 mg (67.3 %) of a green powder

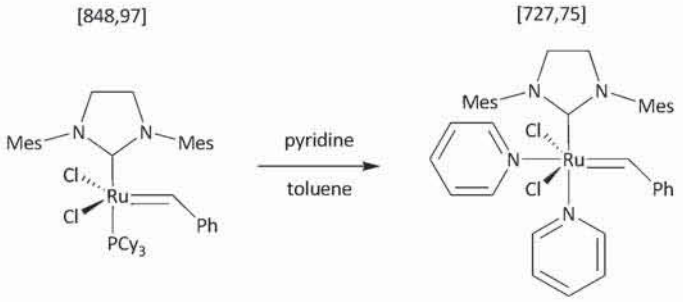

Figure 5.3: Synthesis of $(H_2IMes)(py_2)(Cl)_2Ru{=}CHPh$ (Grubbs catalyst 3rd generation).

5.2.4 Synthesis of poly(bicyclo[2.2.1]hept-5-ene-2,3-dicarboxylic-bis-(4-thiocyanatomethyl)benzyl ester)

To a solution of 250 mg (0.495 mmol, 100 equiv.) of (±)endo,exo-bi-cyclo[2.2.1]-hept-5-ene-2,3-dicarboxylic-bis-(4-thiocyanatomethyl)benzyl ester in 2.5 mL anhydrous THF, 3.61 mg (0.00495 mmol, 1 equiv.) of the initiator $(H_2IMes)(py_2)(Cl)_2Ru{=}CHPh$ dissolved in 1.5 mL anhydrous THF were added at room temperature. The polymerization was monitored by TLC (cyclohexane / ethyl acetate 2/1). After 3 h the solution was treated with 0.1 mL of ethyl vinyl ether for 15 min and subsequently precipitated into 50 mL of cooled methanol. The light brown polymer was reprecipitated in cooled methanol and dried in vacuo.

Yield: 50 mg (20 %) of light brown powder

GPC (THF): $M_w = 29\,527\ g{\cdot}mol^{-1}$, PDI = 1.33

DSC (2nd cycle, heating rate 10 °C.min^{-1}): T_g = 39.10 °C

^{1}H-NMR (400 MHz, 20 °C, $CDCl_3$) δ 7.2 (s, 8H, Ph), 4.8 - 5.5 (m, 6H, $Nb^{5,6}$, $-CH_2$-O), 4.0 (s, 4H, $-CH_2$-SCN), 2.9 - 3.4 (m, 6H, Nb^{1-4}), 1.3 - 2.1 (m, 2H, Nb^7)

FT-IR (CaF_2, cm^{-1}): 2953, 2928, 2858, 2153, 1731, 1515, 1449, 1424, 1391, 1252, 1169, 1110

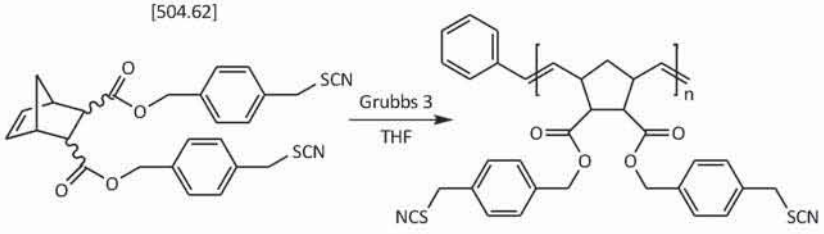

Figure 5.4: Synthesis of poly(bicyclo[2.2.1]hept-5-ene-2,3-dicarboxylic-bis-(4-thiocyanatomethyl)benzyl ester).

5.2.5 Synthesis of poly(4-vinylphenyl 1-naphthoate)

To a solution of 1 g poly(4-vinylphenol) in 10 mL dichloromethane 2.51 mL 1-naphthoyl chloride (16.73 mmol) and 1.35 mL pyridine (16.73 mmol) were added dropwise. The reaction mixture was stirred at room temperature for 60 hours. The polymer was precipitated by dropping the solution into a tenfold excess of cold methanol. The residual 1-naphthoyl chloride was removed by Soxhlet extraction using methanol as extraction solvent. The remaining precipitate was dried at 40 °C in vacuo.

Yield: 1.6 g (70 %) of a white powder

GPC (THF): $M_w = 34\,700\,g.mol^{-1}$, PDI = 2.0

DSC (3rd cycle, heating rate 20 °C.min^{-1}): $T_g = 89.11\,°C$

^{1}H-NMR (400 MHz, 20 °C, $CDCl_3$) δ 6.2 - 9.2 (m, 11H, $Ph^{2,3,5,6}$, Na^{2-8}), 0.9 - 2.3 (m, 3H, -CH-CH_2)

FT-IR (CaF_2, cm^{-1}): 3470, 3050, 2930, 1730, 1593, 1505, 1276, 1238, 1187, 1165, 1118, 984

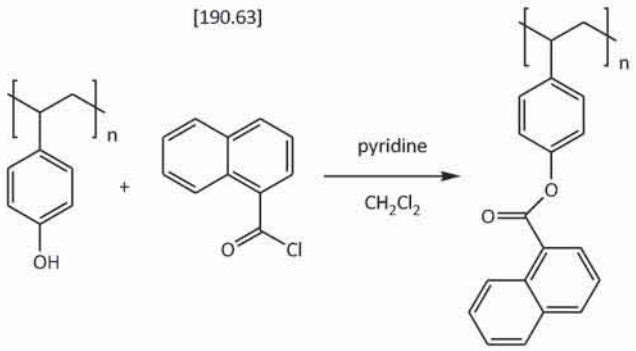

Figure 5.5: Polymer analogous reaction of poly(4-vinylphenol) with 1-naphthoyl chloride.

5.2.6 Synthesis of poly(4-vinylphenyl benzoate)

To a solution of 2 g poly(4-vinylphenol) in 10 mL dichloromethane 3.65 mL benzoyl chloride (33.45 mmol) and 2.70 mL pyridine (33.45 mmol) were added dropwise. The reaction mixture was stirred at room temperature for 60 hours. The polymer was precipitated by dropping the solution into a tenfold excess of cold methanol. The residual benzoyl chloride was removed by Soxhlet extraction using methanol as extraction solvent. The remaining precipitate was dried at 40 °C in vacuo.

Yield: 3.7 g (83 %) of a white powder

GPC (THF): $M_w = 28\,600$ g.mol^{-1}, PDI = 1.6

DSC (2nd cycle, heating rate 10 °C.min^{-1}): $T_g = 145.78$ °C

^{1}H-NMR (400 MHz, 20 °C, $CDCl_3$) δ 8.06 (s, 2H, $Ph^{2',6'}$), 6,38 - 7.62 (m, 7H, $Ph^{3'-5',2,3,5,6}$), 1.29 - 2.03 (m, 3H, -CH-CH_2)

FT-IR (CaF_2, cm^{-1}): 3470, 3035, 2930, 1735, 1600, 1505, 1451, 1276, 1238, 1187, 1166, 1118, 984

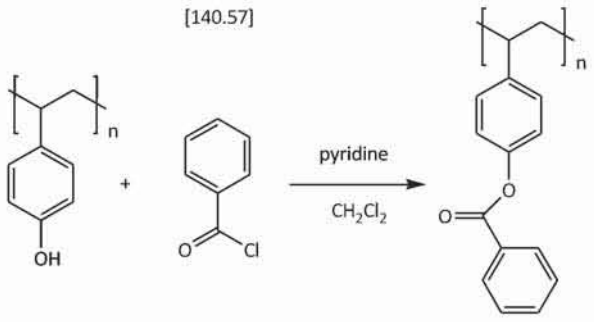

Figure 5.6: Polymer analogous reaction of poly(4-vinylphenol) with benzoyl chloride.

5.2.7 Synthesis of pyrene-1-carbonyl chloride

An amount of 500 mg (2.030 mmol) 1-pyrene carboxylic acid was provided in a Schlenk flask and 4.5 mL (0.062 mmol) thionyl chloride were added dropwise. After refluxing for 20 h excess thionyl chloride was removed using a cooling trap while the remaining liquid was transferred to a round bottom flask and was used directly in the next step without further purification.

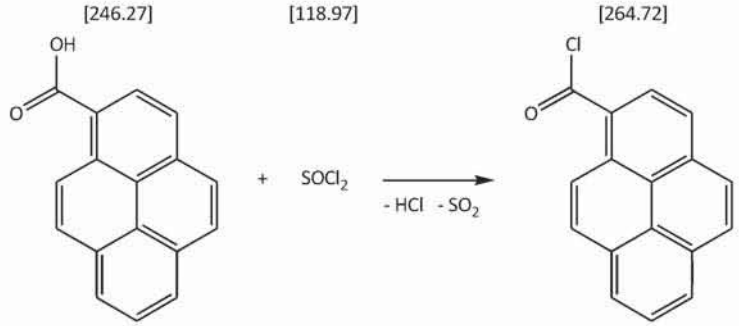

Figure 5.7: Synthesis of pyrene-1-carbonyl chloride.

5.2.8 Synthesis of poly(4-vinylphenyl pyrene-1-carboxylate)

To a solution of 120 mg poly(4-vinylphenol) in 5 mL dichloromethane 537 mg pyrene-1-carbonyl chloride (2.030 mmol; whole amount of product obtained in section 5.2.7) and 0.164 mL pyridine (2.030 mmol) were added dropwise. The reaction mixture was stirred at room temperature for 60 hours. The polymer was precipitated by dropping the solution into a tenfold excess of cold methanol. The remaining precipitate was dried at 40 °C in vacuo.

Yield: 111 mg (34.1 %) of a brown powder

FT-IR (CaF_2, cm^{-1}): 3630, 3362, 3034, 2954, 2620, 1685, 1595, 1511, 1440, 1325, 1260, 1233, 1202, 1168

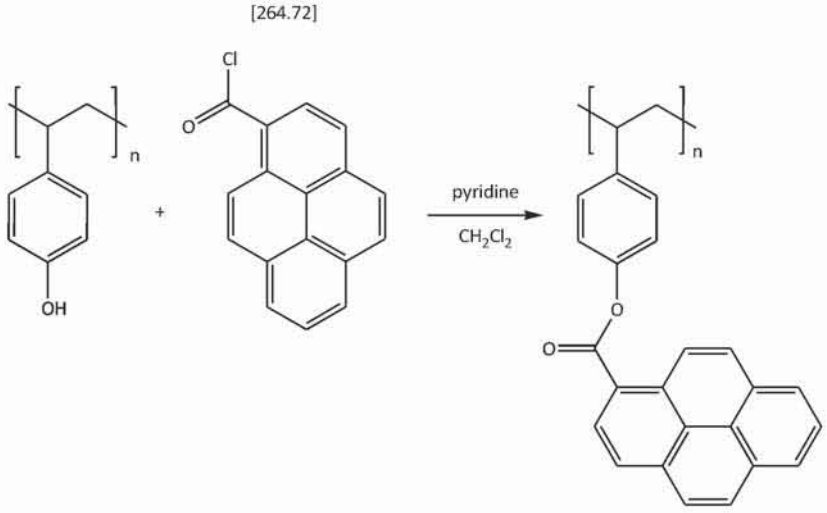

Figure 5.8: Polymer analogous reaction of poly(4-vinylphenol) with pyrene-1-carbonyl chloride.

5.3 Preparing thin polymeric films

5.3.1 Single-layer films

For spectroscopic measurements, thin polymeric films were prepared on CaF_2 plates by spin casting from dichloromethane solutions (15 mg/mL). For photolithographic experiments the polymers were filtered through a 0.45 μm polyamide filter and then coated on CaF_2 plates or silicon wafers from solutions of 30 mg/mL dichloromethane at 1000 rpm for 60 s.

5.3.2 Dual-layer films

In the dual-layer assembly a thin coverglass for conventional optical microscopy was used as a substrate (thickness about 100 μm). The glass platelet is transparent for light above 300 nm wavelength and provides a non-photoreactive interface between the two photosensitive polymeric layers. PVP-**BZ** and PVP-**NA** were spin-cast individually from 15 mg/mL dichloromethane solutions on each side of the substrate.

5.3.3 Thin films in electroluminescent devices

Baytron P (poly(3,4-ethylene dioxythiophene) / poly(styrene sulphonate), aqueous suspension) was spun onto the indium tin oxide (ITO) coated glass after filtration through a 0.45 μm polyamide filter. The following spin-coating parameters were used: 3800 rpm for 10 s and 2700 rpm for 50 s. The PFO/PNOR-**SCN** 4:6 blend was then spun onto the PEDOT/PSS layer from a 10 mg/mL chloroform solution at 1000 rpm for 60 s.

5.4 Photolithographic patterning

Photolithographic patterning was performed with a mask aligner (model MJB4 from SUSS, Germany, resolution 1 μm) using a 500 W HgXe lamp equipped with a filter transmissive either for the wavelength range from 235 nm to 265 nm or for the range from 270 nm to 353 nm.

The photoreactive films, which have been prepared on CaF_2 platelets before, were patterned by using 4 cycles of 5 min illumination time and a 30 s cooling period after each cycle.

The dual-layer patterning was performed by using the following illumination parameters: 4 cycles of 5 min irradiation for the top layer consisting of PVP-**BZ** (235 nm - 265 nm) and 10 cycles of 5 min irradiation for the bottom layer consisting of PVP-**NA** (300 nm - 353 nm). After each cycle a 30 s cooling period was applied to avoid overheating of the sample. For the photolithographic patterning of PVP-**NA** a coverglass was used in addition to the filter transmissive (270 nm - 353 nm) on the top of the assembly in order to provide light with $\lambda \geq 300$ nm.

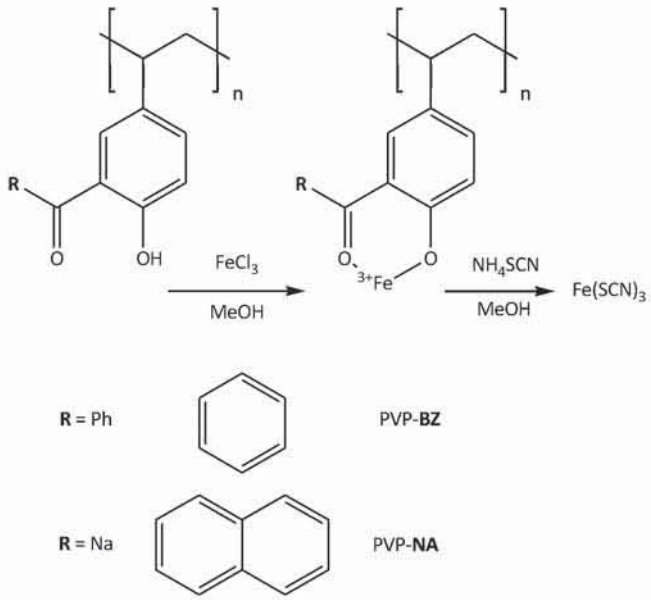

Figure 5.9: Reaction of *o*-hydroxyketones with Fe^{3+} followed by treatment with NH_4SCN.

5.5 Selective post-modification reactions

5.5.1 Post-modification with $FeCl_3$ and NH_4SCN

A thin film of PVP-**NA** was illuminated using an ozone free low pressure Hg lamp (Hereaus Noblelight, 254 nm) for 5 min and was then immersed in a solution of $FeCl_3$ in methanol for two hours, resulting in a slightly yellowish film. The immobilization of Fe^{3+} ions was proven by reaction with NH_4SCN in a solution of methanol, which led to the formation of a deeply red-colored iron(III) thiocyanate complex.

5.5.2 Post-modification with fluorescent dyes

In this work, several fluorescent dyes were used as reactants in post-modifications of thin polymeric films after irradiation with UV light. Table 5.2 gives an overview of all dyes used in different experiments.

Dansyl chloride, Rhodamine B isothiocyanate and $Ru(bpy)_2$(phen-5-isothiocyanate)$(PF_6)_2$ were used for selective surface functionalization in the dual-layer patterning experiments while 2-aminoacridone and $Ru(bpy)_2(phen\text{-}5\text{-}NH_2)(PF_6)_2$,

Table 5.2: List of fluorescent dyes.

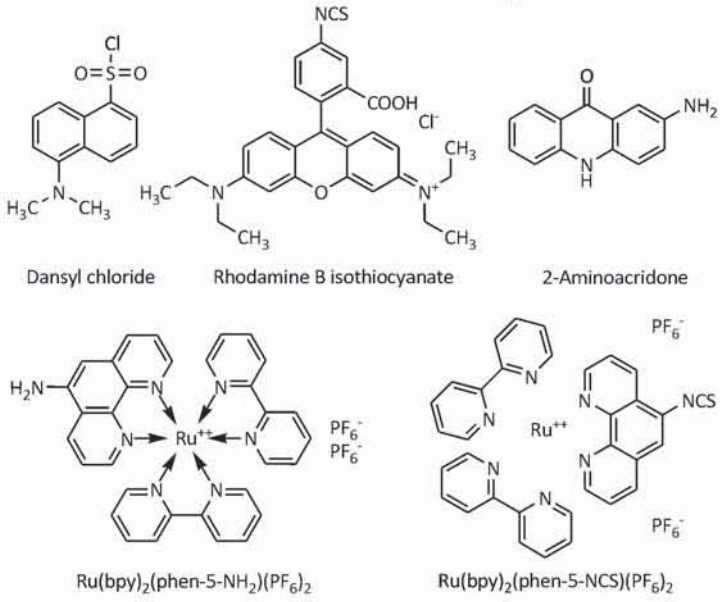

a green and a red fluorescent dye, were used for color-tuning of PFO-based OLEDs.

Irradiated films of PVP-**BZ** and PVP-**NA** undergo a series of reactions, i.e., the reaction of hydroxyl groups with sulfonic acid chlorides. To demonstrate this, dansyl chloride was used, a fluorescent dye. After 20 min UV illumination (HEREAUS Noblelight, 254 nm) of a film of PVP-**BZ**, the sample was developed with a solution of dansyl chloride and triethylamine in acetonitrile for 2 h. The aromatic hydroxyl groups react readily with the sulfonic acid chloride to give the corresponding sulfonic acid ester as displayed in Figure 5.10.

Immobilizing molecules bearing isothiocyanate groups can also be used for selective surface functionalization of the illuminated areas. For this purpose, a Ruthenium red-based fluorescent dye was used. An irradiated film of PVP-**BZ** (illumination time: 30 min; ozone free low pressure Hg lamp, 254 nm) was treated with a solution of $Ru(bpy)_2(phen\text{-}5\text{-}NCS)(PF_6)_2$ and triethylamine in acetonitrile for 2 h. The aromatic hydroxyl groups react readily with the isothiocyanate groups to give a derivative of carbamo thioate, as shown in Figure 5.11.

The thiocyanate groups in PNOR-**SCN** undergo a conversion to isothiocyanate groups when exposed to UV light. These reactive groups easily form

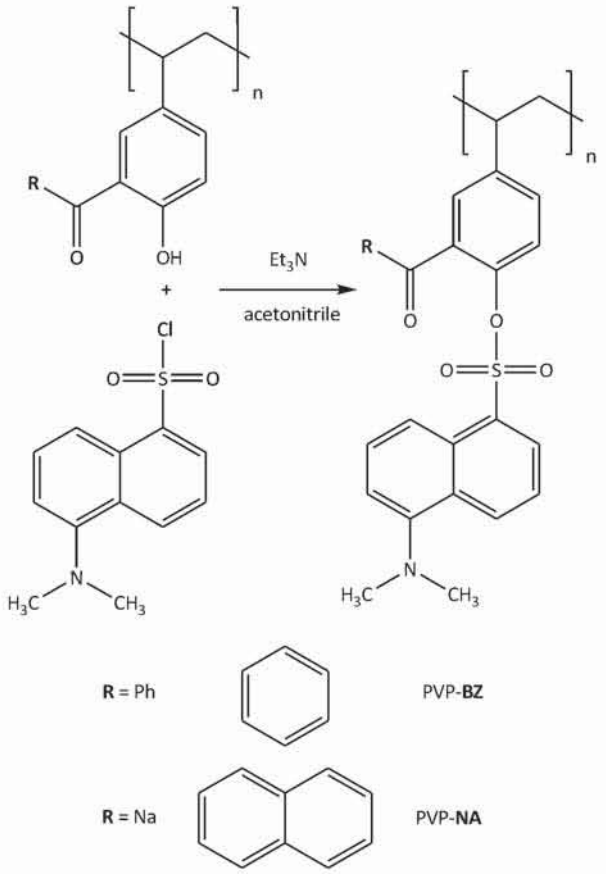

Figure 5.10: Reaction of *o*-hydroxyketones with dansyl chloride under formation of the corresponding sulfonic acid ester.

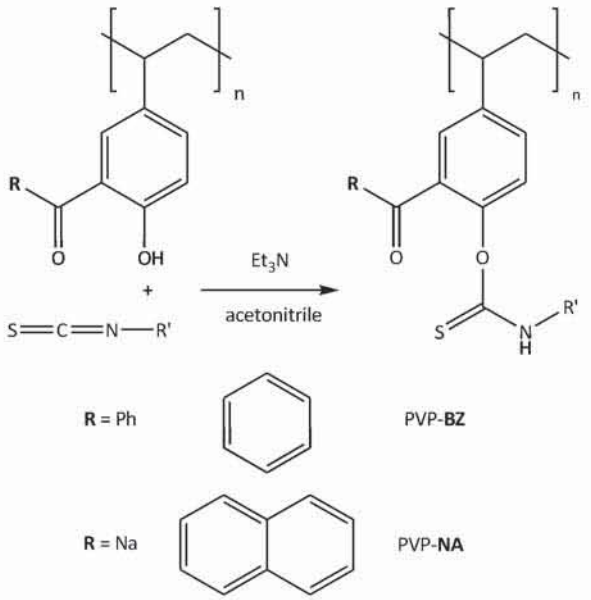

Figure 5.11: Reaction of *o*-hydroxyketones with isothiocyanate groups to give a derivative of carbamo thioate.

a thiourea derivative by treatment with propylamine, which has already been demonstrated in Figure 3.20. This reaction can be adopted by the use of fluorescent dyes bearing amino groups. Therefore, thin films of PNOR-**SCN** (or their blends with PFO, respectively) were illuminated 2 h using a medium pressure Hg lamp (100 W, from NEWPORT, model 66990) equipped with a filter for 254 nm and subsequently exposed to a solution of 5 mg dye in 4 mL acetonitrile, containing a catalytic amount of triethylamine, for 3 h.

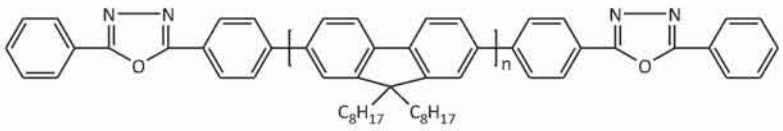

ADS429BE

Figure 5.12: Poly(9,9-dioctylfluorenyl-2,7-diyl) end capped with 2,5-diphenyl-1,2,4-oxadiazole.

Table 5.3: Light emitting homopolymer for OLED & PLED devices (data given by producer).

Technical data of ADS429BE	
Appearance:	yellow fiber or flake
Molecular Weight:	40 000 – 120 000
Absorption maximum:	390 nm
Photoluminescence maximum:	410 nm
Storage:	under N_2 atmosphere

5.6 Fabrication of the OLED

In the fabricated OLEDs a polyfluorene derivative, purchased from American Dye Source Inc., was used. Figure 5.12 shows its chemical structure. The polymer emits blue light as demonstrated by fluorescence spectroscopy in Figure 3.27.

ADS429BE is Poly(9,9-dioctylfluorenyl-2,7-diyl) end capped with 2,5-diphenyl-1,2,4-oxadiazole. It is highly soluble in toluene, tetrahydrofuran, and chlorobenzene. ADS429BE can be used for fabrication of light emitting displays, biosensors, as well as many other applications. Its major properties are listed in Table 5.3.

The fabrication of a polymer light emitting device required several steps. The basic composition is shown in Figure 5.13. First, the ITO coated glass substrate had to be cleaned by treatment with isopropyl alcohol in an ultrasonic bath for 30 min.

Next, the conductive and the emissive layers were applied via spin-casting. Baytron P (poly(3,4-ethylene dioxythiophene) / poly(styrene sulphonate), aqueous suspension) was spun onto the indium tin oxide (ITO) coated glass after filtration through a 0.45 µm polyamide filter. The following spin-coating parameters were used: 3800 rpm for 10 s and 2700 rpm for 50 s. The PFO/PNOR-**SCN** 4:6 blend was then spun onto the PEDOT/PSS layer from a 10 mg/mL chloro-

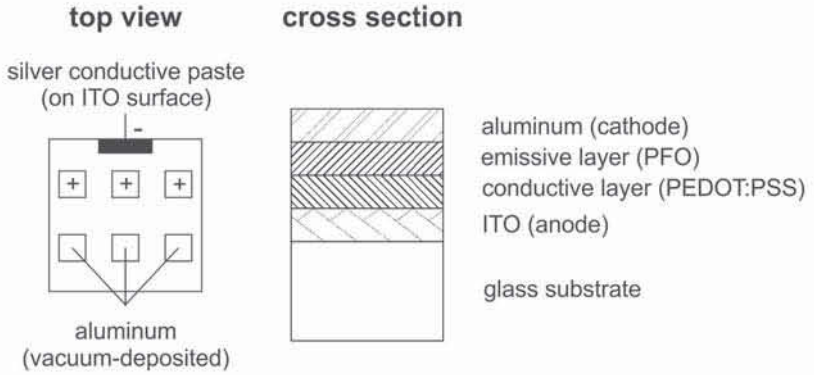

Figure 5.13: Basic composition and cross-sectional view of an OLED.

form solution at 1000 rpm for 60 s.

Finally, on top of this device a layer of aluminum (contact electrode) was deposited by thermal evaporation using a BALZERS MED010. The devices were tested under nitrogen atmosphere in a glovebox.

Bibliography

[1] **E. Menard, et al.** Micro- and Nanopatterning Techniques for Organic Electronic and Optoelectronic Systems. *Chem. Rev.* 2007, **107**, 1117-1160.

[2] **G. Gustafsson, et al.** Flexible light-emitting diodes made from soluble conducting polymers. *Nature.* 1992, **357**, 477-479.

[3] **T. R. Hebner, et al.** Ink-jet printing of doped polymers for organic light emitting devices. *Appl. Phys. Lett.* 1998, **72**, 519-521.

[4] **J. Bharathan, and Y. Yang**. Polymer electroluminescent devices processed by inkjet printing: I. Polymer light-emitting logo. *Appl. Phys. Lett.* 1998, **72**, 2660-2662.

[5] **R. H. Friend, et al.** Electroluminescence in conjugated polymers. *Nature.* 1999, **397**, 121-128.

[6] **C. J. Brabec, N. S. Sariciftci, and J. C. Hummelen**. Plastic Solar Cells. *Adv. Funct. Mater.* 2001, **11**, 15-26.

[7] **B. Kannan, K. Castelino, and A. Majumdar**. Design of Nanostructured Heterojunction Polymer Photovoltaic Devices. *Nano Lett.* 2003, **3**, 1729-1733.

[8] **N. Stutzmann, R. H. Friend, and H. Sirringhaus**. Self-Aligned, Vertical-Channel, Polymer Field-Effect Transistors. *Science.* 2003, **299**, 1881-1884.

[9] **S. Möller, et al.** A polymer/semiconductor write-once read-many-times memory. *Nature.* 2003, **426**, 166-169.

[10] **P. S. Ramanujam, et al.** Physics and technology of optical storage in polymer thin films. *Synthetic metals.* 2001, **124**, 145-150.

[11] **A. Lex, et al.** Photosensitive polynorbornene containing the benzyl thiocyanate group - Synthesis and patterning. *J. Mol. Catal. A: Chem.* 2006, **254**, 174-179.

[12] **G. Langer, et al.** UV-induced processes in PVBT. *Macromol. Chem. Phys.* 2001, **202**, 3459-3467.

[13] **T. Kavc, et al.** Phase gratings in photoreactive polymers: a way to optically pumped organic lasers. *Monatsh. Chem.* 2001, **132**, 531-50.

[14] **J. C. Anderson, and C. B. Reese**. A photo-induced rearrangement involving aryl participation. *Tetrahedron Lett.* 1961, **3**, 1-4.

[15] **C. E. Kalmus, and D. M. Hercules**. A mechanistic study of the photo-Fries rearrangement of phenyl acetate. *J. Am. Chem. Soc.* 1974, **96**, 449-456.

[16] **M. A. Miranda, and F. Galindo**. Photo Fries Reaction and Related Processes. [ed.] W.M. Horspool. *CRC Handbook of Organic Photochemistry and Photobiology*. 2nd. Boca Raton : CRC Press, 2004.

[17] **S. Lochbrunner, et al.** Real time observation of the photo-Fries rearrangement. *J. Chem. Phys.* 2004, **120**, 11634-11639.

[18] **S. Grimme**. MO-theoretical investigation on the photodissociation of carbon-oxygen bonds in aromatic compounds. *Chem. Phys.* **163**, 313-330.

[19] **T. Mori, et al.** Isolation of cyclohexadienone intermediates in the photo-Fries rearrangement of 2,4-dimethylnaphth-1-yl and 1,4-dimethylnaphth-2-yl 2,4,6-trimethylbenzoates. *Chem. Lett.* 2004, **33**, 254-257.

[20] **S. K. L. Li, and J. E. Guillet**. Studies of the Photo-Fries Reaction in Solid Poly(phenyl acrylate). *Macromolecules.* 1977, **10**, 840-844.

[21] **R. A. Finnegan, and D. Knudsen**. Photochemical studies, VII. Solvent effects on the photolysis of aryl esters: fries rearrangement vs. decarboxylation. *Tetrahedron Lett.* 1968, **9**, 3429-3432.

[22] **W. Gu, D. J. Abdallah, and R. G. Weiss**. Conformational control of photoinduced decarboxylation of simple aryl esters.: Enhancement by templating effects in polyethylene films. *J. Photochem. Photobiol. A: Chem.* 2001, **139**, 79-87.

[23] **S. Temmel, T. Höfler, and W. Kern**. Modulation of the surface properties of reactive polymers by photo-Fries rearrangement. [ed.] K. L. Mittal. *Contact Angle, Wettability and Adhesion*. 2008, **5**, 229-238.

[24] **G. E. Gillberg-LaForce, et al.** *Polymeric direct imaging holographic compositions*. 5128223 [ed.] Hoechst Celanese Corp. 1992. US Patent.

[25] **T. Grießer, et al.** Refractive Index Modulation of Polymeric Materials via the Photo Fries Rearrangement of Aryl Esters using different Wavelengths. *J. Mater. Chem.* 2009, **19**, 4557-4566.

[26] **D. Bellus, et al.** Photoumlagerung und Photoabbau des Poly(4-benzoyloxystyrols) und Poly(p-kresylacrylats). *J. Polym. Sci.* 1969, **22**, 629-643.

[27] **J. E. Guillet, et al.** Photophysics and Photochemistry of Naphthly Ester Polymers in Solution. *Macromolecules*. 1980, **13**, 1138–1143.

[28] **J. M. J. Frechet, et al.** Poly(n-formyloxystyrene): synthesis and radiation induced decarboxylation. *Macromolecules*. 1985, **18**, 317-321.

[29] **J. L. Hérisson, and Y. Chauvin**. Catalysis of olefin transformations by tungsten complexes. II. Telomerization of cyclic olefins in the presence of acyclic olefins. *Makromolekul. Chem.* 1971, **141**, 161–176.

[30] **T. Grießer**. *Anwendung der Photo-Fries-Reaktion zur Oberflächenmodifizierung*. Graz University of Technology : Institute for Chemistry and Technology of Materials, 2008.

[31] **K. P. C. Vollhardt, and N. E. Schore**. *Organic Chemistry - Structure and Function*. New York : W. H. Freeman and Company, 2002. 579-588.

[32] **M. Pope, H. P. Kallmann, and P. Magnante**. Electroluminescence in organic crystals. *J. Chem. Phys.* 1963, **38**, 2042-2043.

[33] **R. H. Partridge**. Electro-luminescence from polyvinylcarbazole films. 1. Carbazole cations. *Polymer*. 1983, **24**, 733–738.

[34] **L. Akcelrud**. Electroluminescent polymers. *Prog. Polym. Sci.* 2003, **28**, 875–962.

[35] **D. Neher, and F. Jaiser**. *Licht in und aus Plastik: Optoelektronik mit Polymeren*. Potsdam : Institut für Physik und Astronomie der Universität Potsdam.

[36] **C. W. Tang, and S. A. VanSlyke**. Organic electroluminescent diodes. *Appl. Phys. Lett.* 1987, **51**, 913-915.

[37] **M. A. Baldo, M. E. Thompson, and S. R. Forrest**. High-efficiency fluorescent organic light-emitting devices using a phosphorescent sensitizer. *Nature*. 2000, **403**, 750-753.

[38] **C. D. Müller, et al.** Multi-colour organic light-emitting displays by solution processing. *Nature*. 2003, **421**, 829-833.

[39] **M. C. Choi, Y. Kim, and C. S. Ha**. Polymers for flexible displays: From material selection to device applications. *Prog. Polym. Sci.* 2008, **33**, 581–630.

[40] **A. Weber, et al.** Thin Glass-Polymer Systems as Flexible Substrates for Displays. *SID Symposium Digest of Technical Papers*. 2002, **33**, 53-55.

[41] **H. S. Shin, et al.** 4.1 inch Top-Emission AMOLED on Flexible Metal Foil. *SID Symposium Digest of Technical Papers*. 2005, **36**, 1642-1647.

[42] **H. Antoniadis**. *An Overview of OLED Display Technology*. San Jose, CA : OSRAM Opto Semiconductors Inc., 2003.

[43] **G. P. Crawford**. *Flexible flat panel display technology*. New York : Wiley, 2005.

[44] **J. Lewis**. Material challenge for flexible organic devices. *Mater. Today*. 2006, **9**, 38–45.

[45] **S. E. Burns, et al.** Flexible active-matrix displays. *SID Symposium Digest of Technical Papers*. 2005, **36**, 19-21.

[46] **G. H. Gelinck, et al.** Rollable QVGA active matrix displays based on organic electronics. *SID Symposium Digest of Technical Papers*. 2005, **36**, 6-9.

[47] **P. Gómez-Romero, and C. Sánchez**. *Functional hybrid materials*. Weinheim : Wiley-VCH, 2004, 240.

[48] **H. Kim, et al.** Anode material based on Zr-doped ZnO thin films for organic light-emitting diodes. *Appl. Phys. Lett.* 2003, **83**, 3809-3811.

[49] **Y. M. Lu, S. I. Tsai, and C. M. Chang**. Highly conductive and transparent Ti-doped zinc oxide thin films. *Mat. Res. Soc. Symp. Proc.* 2003.

[50] **E. Fortunato, et al.** New developments in gallium doped zinc oxide deposited on polymeric substrates by RF magnetron sputtering. *Surf. Coat. Technol.* 2004, **180-181**, 20-25.

[51] **K. Müllen, and U. Scherf**. *Organic light-emitting devices: Synthesis, properties, and applications*. Weinheim : Wiley-VCH, 2006, 153.

[52] **E. B. Namdas, et al.** Simple color tuning of phosphorescent dendrimer light emitting diodes. *Appl. Phys. Lett.* 2005, **86**, 161104.

[53] **M. Vasilopoulou, et al.** Tuning the Emitting Color of Organic Light-Emitting Diodes Through Photochemically Induced Transformations: Towards Single-Layer, Patterned, Full-Color Displays and White-Lighting Applications. *Adv. Funct. Mater.* 2007, **17**, 3477-3485.

[54] **G. Trattnig, et al.** Tuning the emission color of conjugated organic materials by photochemical reactions. *Synthetic Metals.* 2003, **137**, 1027-1028.

[55] **A. J. Elias**. *A Collection of Interesting General Chemistry Experiments*. Hyderabad : Universities Press (India), 2002, 54.

[56] **Z. R. Li, and H. Meng**. *Organic light-emitting materials and devices*. Boca Raton : CRC Press, 2007, 415-417.

[57] **F. Vögtle, N. Werner, and G. Richardt**. *Dendritische Moleküle: Konzepte, Synthesen, Eigenschaften, Anwendungen*. Wiesbaden : Teubner, 2007, 188.

[58] *Concepts in Fluorescence Microscopy*. [online] Nikon Instruments, Inc. [cited: 2010-11-14.] http://www.microscopyu.com/articles/fluorescence/-fret/images/fretintrofigure1.jpg.

[59] **T. Förster**. *Naturwissenschaften*. 1946, **6**, 166-175.

[60] **R. Clegg**. The Vital Contributions of Perrin and Förster. *Biophotonics International*. 2004, September.

[61] **A. Dogariu, et al.** Time-resolved Förster energy transfer in polymer blends. *Synth. Met.* 1999, **100**, 95-100.

[62] **D. B. Williams, and C. B. Carter**. *Transmission electron microscopy*. New York : Plenum Press, 1996, 100.

[63] **D. J. Whitehouse**. *Surfaces and their measurement*. New York : Taylor & Francis, 2002, 203.

[64] **D. A. Timuçin, and J. D. Downie**. *Holographic Optical Data Storage*. s.l. : NASA Ames Research Center, 2000.

[65] **L. Dhar, K. Curtis, and T. Fäcke**. Holographic data storage: Coming of age. *Nature Photonics*. 2008, **2**, 403-405.

[66] **Y. Kawata, M. Nakano, and S. C. Lee**. Three-dimensional optical data storage using three-dimensional optics. *Opt. Eng.* 2001, **40**, 2247-2254.

[67] **M. Ishikawa, et al.** Reflection-type confocal readout for multilayered optical memory. *Opt. Lett.* 1998, **23**, 1781-1783.

[68] **D. K. Owens, and R. C. Wendt**. Estimation of the Surface Free Energy of Polymers. *J. Appl. Polym. Sci.* 1969, **13**, 1741-1747.

[69] **W. Rabel**. Einige Aspekte der Benetzungstheorie und ihre Anwendung auf die Untersuchung und Veränderung der Oberflächeneigenschaften von Polymeren. *Farbe und Lacke*. 1971, **77**, 997-1005.

[70] **W. Göpel, and C. Ziegler**. *Einführung in die Materialwissenschaften: Physikalisch-chemische Grundlagen und Anwendung*. s.l. : Teubner Verlag, 1996, 131.

[71] **F. M. Fowkes**. Attractive forces at interfaces. *Ind. Eng. Chem.* 1964, **56**, 40-52.

[72] **G. Socrates**. *Infrared Characteristic Group Frequencies*. Chichester : John Wiley & Sons, 1998.

[73] **T. Höfler, et al**. UV reactive polymers for refractive index modulation based on the photo-Fries rearrangement. *Polymer*. 2007, **48**, 1930-1939.

[74] **I. Assaid, D. Posq, and I. Hardy**. Improvements of the Poly(vinyl cinnamate) Photoresponse in Order to Induce High Refractive Index Variations. *Phys. Chem. B*. 2004, **108**, 2801-2806.

[75] **A. Nagata, et al.** Refractive index decrease during photocrosslinking in photopolymers suitable for holographic recording. *Macromol. Rapid Commun.* 1997, **18**, 191-196.

[76] **T. Grießer, et al.** Photolithographic Patterning of Polymer Surfaces Using the Photo-Fries Rearrangement: Selective Postexposure Reactions. *Chem. Mater.* 2007, **19**, 3011-3017.

[77] **J. Kido, et al.** White light-emitting organic electroluminescent devices using the poly(N-vinylcarbazole) emitter layer doped with three fluorescent dyes. *Appl. Phys. Lett.* 1994, **64**, 815-817.

[78] **M. D. McGehee, et al.** Narrow Bandwidth Luminescence from Blends with Energy Transfer from Semiconducting Conjugated Polymers to Europium Complexes. *Adv. Mater.* 1999, **11**, 1349-1354.

[79] **M. Leclerc**. Polyfluorenes: Twenty years of progress. *J. Polym. Sci. A: Polym Chem.* 2001, **39**, 2867-2873.

[80] **S. Becker, et al.** Optimisation of polyfluorenes for light emitting applications. *Synth. Met.* 2001, **125**, 73-80.

[81] **F. I. Wu, et al.** Enhancing the thermal and spectral stabilities of polyfluorene-based blue-light-emitting materials by incorporating pendent spiro-cycloalkyl groups. *Polymer.* 2004, **45**, 4257-4263.

[82] **C. Ego, et al.** Triphenylamine-Substituted Polyfluorene - A Stable Blue-Emitter with Improved Charge Injection for Light-Emitting Diodes. *Adv. Mater.* 2002, **14**, 809-811.

[83] **A. Pogantsch, et al.** Polyfluorenes with Dendron Side Chains as the Active Materials for Polymer Light-Emitting Devices. *Adv. Mater.* 2002, **14**, 1061-1064.

[84] **F. I. Wu, D. S. Reddy, and C. F. Shu**. Novel Oxadiazole-Containing Polyfluorene with Efficient Blue Electroluminescence. *Chem. Mater.* 2003, **15**, 269-274.

[85] **C. F. Shu, R. Dodda, and F. I. Wu.** Highly Efficient Blue-Light-Emitting Diodes from Polyfluorene Containing Bipolar Pendant Groups. *Macromolecules.* 2003, **36**, 6698-6703.

[86] **J. Kido, H. Shionoya, and K. Nagai**. Single-layer white light-emitting organic electroluminescent devices based on dye-dispersed poly(N-vinylcarbazole). *Appl. Phys. Lett.* 1995, **67**, 2281-2283.

[87] **T. Virgili, D. G. Lidzey, and D. D. C. Bradley**. Efficient Energy Transfer from Blue to Red in Tetraphenylporphyrin-Doped Poly(9,9-dioctylfluorene) Light-Emitting Diodes. *Adv. Mater.* 2000, **12**, 58-62.

[88] **N. S. Cho, et al.** Synthesis, Characterization, and Electroluminescence of New Conjugated Polyfluorene Derivatives Containing Various Dyes as Comonomers. *Macromolecules.* 2004, **37**, 5265-5273.

[89] **Q. Peng, et al.** Synthesis and Characterization of New Red-Emitting Polyfluorene Derivatives Containing Electron-Deficient 2-Pyran-4-ylidene−Malononitrile Moieties. *Macromolecules.* 2004, **37**, 260-266.

[90] **H. J. Su, et al.** Color Tuning of a Light-Emitting Polymer: Polyfluorene-Containing Pendant Amino-Substituted Distyrylarylene Units. *Adv. Funct. Mater.* 2005, **15**, 1209-1216.

[91] **C. Buchgraber, et al.** Luminescent Copolymer for Applications in Multicolor-Light-Emitting Devices. *J. Polym. Sci. A: Polym. Chem.* 2006, **44**, 4317-4327.

[92] **H. E. Gottlieb, V. Kotlyar, and A. Nudelman**. NMR Chemical Shifts of Common Laboratory Solvents as Trace Impurities. *J. Org. Chem.* 1997, **21**, 7512-7515.

[93] **C. Slugovc, S. Demel, and F. Stelzer**. Ring opening metathesis polymerisation in donor solvents. *Chem. Comm.* 2002, 2572-2573.

[94] **M. S. Sanford, J. A. Love, and R. H. Grubbs**. A Versatile Precursor for the Synthesis of New Ruthenium Olefin Metathesis Catalysts. *Organometallics.* 2001, **20**, 5314-5318.

[95] **H. B. Shizuka**. Photochemistry of Acetanilide. III. The Secondary Processes in the Photochemical Reaction. *Bull. Chem. Soc. Jpn.* 1969, **42**, 57-65.

List of Figures

List of Tables

List of Abbreviations

CFM	confocal fluorescence microscopy
CTE	coefficient of thermal expansion
CVD	chemical vapor deposition
DSC	differential scanning calorimetry
DMSO	dimethyl sulfoxide
ETL	electron transport layer
FMS	fluorescent multi-layer storage
FOLED	flexible organic light emitting diode
FRET	Förster resonance energy transfer
FT-IR	Fourier transform spectroscopy
GPC	gel permeation chromatography
HOMO	highest occupied molecular orbital
HTL	hole transport layer
ITO	indium tin oxide
LED	light emitting diode
LUMO	lowest unoccupied molecular orbital
M_n	number average of molar mass
M_w	weight average of molar mass
NA	numerical aperture
OLED	organic light emitting diode
PAG	photoacid generator
PDI	polydispersity index
PEEK	polyether ether ketone
PEDOT:PSS	mixture of poly(3,4-ethylenedioxythiophene) and poly(styrenesulfonate)
PEN	poly(ethylene naphthalate)
PET	poly(ethylene terephthalate)
PFO	polyfluorene
PLED	polymer light emitting diode
PNOR-**SCN**	poly(bicyclo[2.2.1]hept-5-ene-2,3-dicarboxylic-bis-(4-thiocyanatomethyl)benzyl ester
PVP	poly(4-vinyl phenol)
PVP-**BZ**	poly(4-vinylphenyl benzoate)

PVP-**NA**	poly(4-vinylphenyl 1-naphthoate)
PVP-**PY**	poly(4-vinylphenyl pyrene-1-carboxylate)
ROMP	ring-opening metathesis polymerization
SEC	size exclusion chromatography
SMOLED	small molecule organic light emitting diode
SNR	signal-to-noise ratio
STM	scanning tunneling microscope
TCO	transparent conductive oxide
T_g	glass transition temperature
THF	tetrahydrofuran
TLC	thin layer chromatography
UV	ultraviolet

Affidavit

I declare in lieu of oath, that I wrote this thesis and performed the associated research myself, using only literature cited in this volume.

Eidesstattliche Erklärung

Ich erkläre an Eides statt, dass ich diese Arbeit selbstständig verfasst, andere als die angegebenen Quellen und Hilfsmittel nicht benutzt und mich auch sonst keiner unerlaubten Hilfsmittel bedient habe.

Leoben, 2010-11-25 _____

Index